UNIVERSITA' DEGLI STUDI DI NAPOLI

"FEDERICO II"

Dipartimento di Scienze Biomediche Avanzate

DOTTORATO DI RICERCA IN IMAGING MOLECOLARE

XXVIII ciclo

Coordinatore: Prof. Alberto Cuocolo

Contrast-enhanced ultrasound study of Internal Jugular vein blood flow in Multiple Sclerosis patients. Imaging study of cerebral venous system in mouse.

Tutors:

Prof. Marcello Mancini

Prof. Simone Maurea

Dottorando:

Monica Ragucci

Dedication

This thesis work is dedicated to my husband, Enzo, who has been a constant source of support and encouragement during the challenges of graduate school and life. I am truly thankful for having you in my life.

This work is also dedicated to my parents, Massimo e Pompea, who have always loved me unconditionally and whose good examples have taught me to work hard for the things that I aspire to achieve.

Abstract 1

Chapter 1: The cerebral venous system 2

1.1 Intracranial venous system 2

1.1.1 Superficial venous system 2

1.1.2 Deep venous system 4

1.1.3 Dural sinuses 5

1.2 Extracranial venous system 7

1.3 Physiology 9

Chapter 2: Vascular aspects of Multiple Sclerosis 10

2.1 Introduction 10

2.2 Vascular abnormalities 10

2.2.1 Multiple Sclerosis and ischaemic stroke 10

2.2.2 Cerebral hypoperfusion in Multiple Sclerosis 11

2.2.3 Venous blood drainage in Multiple Sclerosis 12

Chapter 3: Cerebral venous system: Ultrasound tecniques 15

3.1 Transcranial Doppler sonography 15

3.2 Extracranial Doppler sonography 16

3.3 Ultrasound contrast agents 17

Chapter 4: Esperimental studies 19

4.1 Internal Jugular Vein Blood Flow in Multiple Sclerosis Patients and Matched 19

4.1.1 Introduction 19

4.1.2 Material and Methods 20

4.1.3 Results 24

4.1.4 Discussion 27

4.2 Head and Neck Veins of the Mouse 29

4.2.1 Introduction 29

4.2.2 Material and Methods 29

4.2.3 Results 31

4.2.4 Discussion 44

Chapter 5: Conclusion and Perspectives 47

Bibliography 50

Acknowledgements 60

Abstract

The underlying mechanism of the widespread axonal degeneration in Multiple Sclerosis (MS) is not yet fully understood. The patterns of demyelination are different between different subgroups of patients with MS, suggesting that the disease is heterogeneous. It is known that the development of a chronic inflammatory reaction in the brain requires additional factors and that the impairment associated with relapsing-remitting clinical form is primarily caused by inflammation and demyelination, whereas the accumulation of irreversible neurological deficit, typical of the progressive forms, is caused mainly by axonal destruction and neuronal loss. Other mechanisms may contribute in determining brain damage during the course of the disease. One hypothesis is that immune factors interacting with the vascular system may secondarily induce changes in cerebral perfusion that are detectable in both early stage of disease and advanced disease and that may cause neuronal damage. The higher frequency of ischemic stroke in patients with MS may be due to several factors such as inflammation, oxidative stress, and increase of thrombophilic factors such as homocysteine. Recently it has been suggested that alterations of cerebral venous outflow in MS patients could determine perivenular extravasations of erythrocytes, iron overload and activation of the immune response. Vascular dysfunction could be one of the factors involved in the complex pathogenesis of MS. However, available data to support the presence and importance of vascular dysfunction are still insufficient to draw definitive conclusions. A first part of research project was to study the Internal Jugular Veins dynamics in MS patients compared with healthy controls using contrast-enhanced ultrasonography. The patients with MS showed a significantly reduction of wash-out rate compared to healthy controls [22.2% (2.7%-65.9%) vs. 33.4% (16.2%-76.8%); $P<0.005$]. Then we decided to explore the effect of cerebral outflow reduction on cerebral nervous system in experimental animal model. Therefore, the second part of research project was dedicated to the characterization the anatomy of the cerebral veins of the mouse brain using different imaging techniques. This work was preliminary to the development of a mice model of cerebral outflow occlusion to assess the correlations between venous stasis and the development of neurological disease.

Chapter 1

The cerebral venous system

1.1 Intracranial venous system

The cerebral venous system (CVS) is mainly composed of *dural sinuses* and *cerebral veins. The dural sinuses* are valveless venous channels which drain the blood from the brain, situated between the two layers of the dura mater and lined by endothelium. *The cerebral veins* are characterized by extremely thin walls, due to the absence of muscular tissue and absence of valves. They penetrate into the arachnoid membrane and the inner layer of the dura mater, and drain into the cranial venous sinuses. The venous outflow from cerebral hemispheres consists mainly of two different vascular systems:

The superficial (cortical) system reaches dural sinuses by cortical veins and drains blood mainly from cortex and subcortical white matter.

The deep (medullary and subependymal) system drains the deep white and gray matter surrounding the lateral and third ventricles or the basal cistern.

The flow in the superficial cortical veins was directed from the deep to the superficial of the brain whereas the direction of flow of deep vein system was directed from superficial to deep of the brain. (1-6)

1.1.1 Superficial venous system

The superficial venous system comprises the *sagittal sinuses* and *cortical veins (Fig.1).*

The superior sagittal sinus (SSS) starts at the foramen coecum, just anterior to the crista galli. It courses along the gentle curvature of the inner table of the skull, within the leaves of the dura mater, to reach the confluence of sinuses: the torcular Herophili. The sinus receives venous tributaries of the superficial venous system (i.e.superficial cortical veins). Its vascular caliber increased form anterior to posterior, but irregularly because of venous lakes contained within the two layers of the dura mater adjacent to the sinus and because of the penetration of arachnoid villi inside its lumen. The *SSS* is circulating in a more or less laminal way,

accentuated by the existence of longitudinal septa, especially in mid-third portion (4,7). The *torcular Herophili* is the term applied to the dilated extremity of the superior sagittal sinus. It is of irregular form, and is lodged on one side (generally the right) of the internal occipital protuberance. From it the transverse sinus of the same side is derived. It receives also the blood from the occipital sinus, and is connected across the middle line with the commencement of the transverse sinus of the opposite side (8).

The inferior sagittal sinus (ISS) is contained in the posterior half or two-thirds of the free margin of the falx cerebri. It is of a cylindrical form, increases in size as it passes backward, and ends in the straight sinus. It receives several veins from the falx cerebri, and occasionally a few from the medial surfaces of the hemispheres (8).

The cortical veins course along the cortical sulci, drain the cortex and some of the adjacent white matter. The large cortical veins can be identified and according to their locations, cortical venous system can be subdivided into superior, middle and inferior groups. Important veins of superficial cerebral venous system are (9):

- superficial middle cerebral vein
- superior anastomotic vein of Trolard
- vein of Labbé

The superficial middle cerebral vein (SMCV) (also known as the Sylvian vein) usually passes along the Sylvian fissure posteroanteriorly, it collects numerous small tubutaries which drain the opercular areas around the lateral sulcus. It curves anteriorly around the tip of the temporal lobe and drains into the sphenoparietal sinus or cavernous sinus. It may have connections to dural venous sinuses by anastomotic veins:

- to the superior sagittal sinus by the great anastomotic vein of Trolard
- to the transverse sinus by the posterior anastomotic vein of Labbé (9)

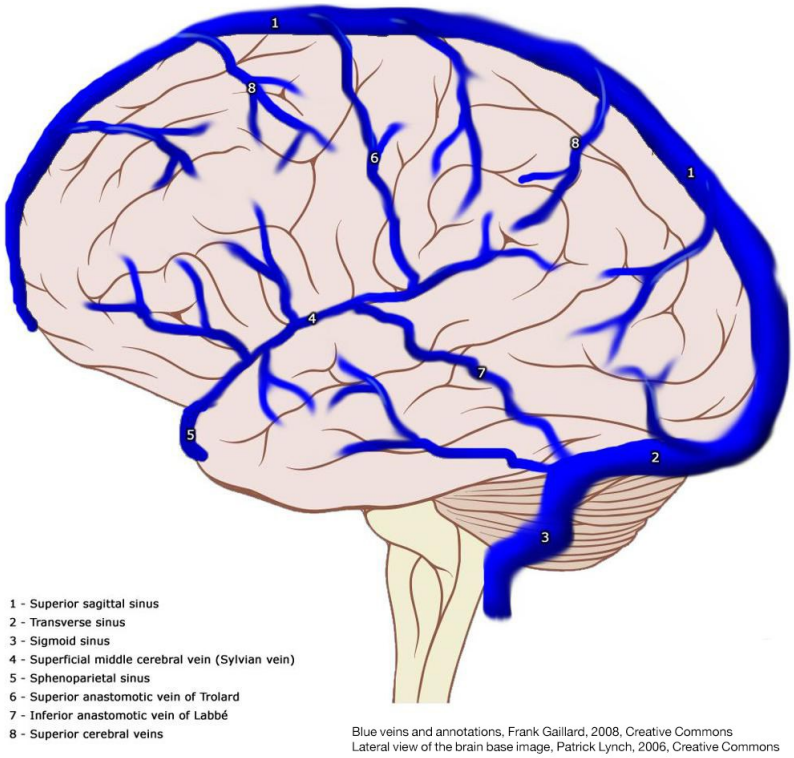

Fig.1 Lateral view of the brain base.

1.1.2 Deep venous system

The principal deep cerebral veins are:

The internal cerebral veins are paired vessels that are situated just off the midline. They are adjacent to each other in the tela choroidea of the roof of the 3rd ventricle for most of their course. Their configuration is therefore that of the roof of the 3rd ventricle. These veins begin at the foramen of Monro, leave the roof of the 3rd ventricle and enter the upper portion of the quadrigeminal cistern, where they join to the great cerebral vein (of Galen), in the posterior incisural space. The main tributary of the internal cerebral vein on each side is the thalamostriate (or terminal) vein (10).

The basal veins (veins of Rosenthal) are paired veins that originate on the medial aspect of the anterior portion of the temporal lobe, near the optic chiasm. They are formed from tributaries arising on the medial surface and temporal horn of the

temporal lobe, from a small anterior cerebral vein that runs adjacent to the anterior cerebral artery, and from the large, deep middle cerebral veins (10).

The deep middle cerebral vein passes through the anterior perforated substance, where it joins anterior cerebral vein to form the anterior segment of the basal vein of Rosenthal. The basal vein passes around the mesencephalon beneath the uncus and hippocampal gyrus. It course parallels, but slightly rostral to the course of the posterior cerebral artery. It usually unites with the two internal cerebral veins and the contralateral basal vein to form the vein of Galen.

The vein of Galen, also known as the great cerebral vein or great vein of Galen, is a short trunk formed by the union of the two internal cerebral veins and basal veins of Rosenthal. It lies in the quadrigeminal cistern. It curves backward and upward around the posterior border of the splenium of the corpus callosum to drain into the straight sinus. It receives numerous tributaries: callosal veins, precentral cerebellar vein superior cerebellar veins, inferior cerebral veins (draining medial inferior temporal lobe) (11).

1.1.3 Dural sinuses

Transverse sinuses, sigmoid sinuses, straight sinus drain deep cerebral veins *(Fig.2)*.

The transverse sinuses (TS) drain the superior sagittal sinus, the occipital sinus and the straight sinus, and empties into the sigmoid sinus, which in turn reaches the jugular bulb. The two transverse sinuses arise at the confluence of the three aforementioned sinuses at the torcular herophili (12).

The sigmoid sinus is the continuation of the transverse sinus (which is similarly variable in size) and becomes the sigmoid sinus as the tentorium ends. It is here that the sinus receives the superior petrosal sinus. It passes inferiorly in an S shaped groove posteromedial to the mastoid air-cells to the jugular foramen, where it ends in the jugular bulb, in the posterior half of the foramen (pars vascularis). It has connections via mastoid and condylar emissary veins with pericranial veins (8).

The straight sinus, therefore, drains the deep venous system through the vein of Galen as well as part of superficial venous system through the ISS. As are all other sinuses, the straight sinus is situated within dural leaves, tentorium cerebelli and falx cerebri. Posteriorly, straight sinus empties into torcular. Another complex network of dural sinuses collects blood along the brain's ventral surface including *the cavernous, superior and inferior petrosal, and sphenoparietal sinuses.The cavernous sinuses* are of irregular form, larger behind than in front, and are placed one on either side of the body of the sphenoid bone, extending from the superior orbital fissure to the apex of the petrous portion of the temporal bone. Each opens behind into the petrosal sinuses. On the medial wall of each sinus is the internal carotid artery, accompanied by filaments of the carotid plexus. The cavernous sinus receives the superior ophthalmic vein through the superior orbital fissure, some of the cerebral veins, and also the small *sphenoparietal sinus*, which courses along the inferior surface of the small wing of the sphenoid. The two sinuses also communicate with each other by means of the *anterior and posterior intercavernous sinuses. The anterior* passes in front of the hypophysis, *the posterior* behind it, and they form with the cavernous sinuses a venous circle (circular sinus) around the hypophysis. *The superior petrosal sinus* connects the cavernous with the transverse sinus. *The inferior petrosal sinus* is situated in the inferior petrosal sulcus formed by the junction of the petrous part of the temporal with the basilar part of the occipital. It begins in the postero-inferior part of the cavernous sinus, and, passing through the anterior part of the jugular foramen, ends in the superior bulb of the internal jugular vein (4).

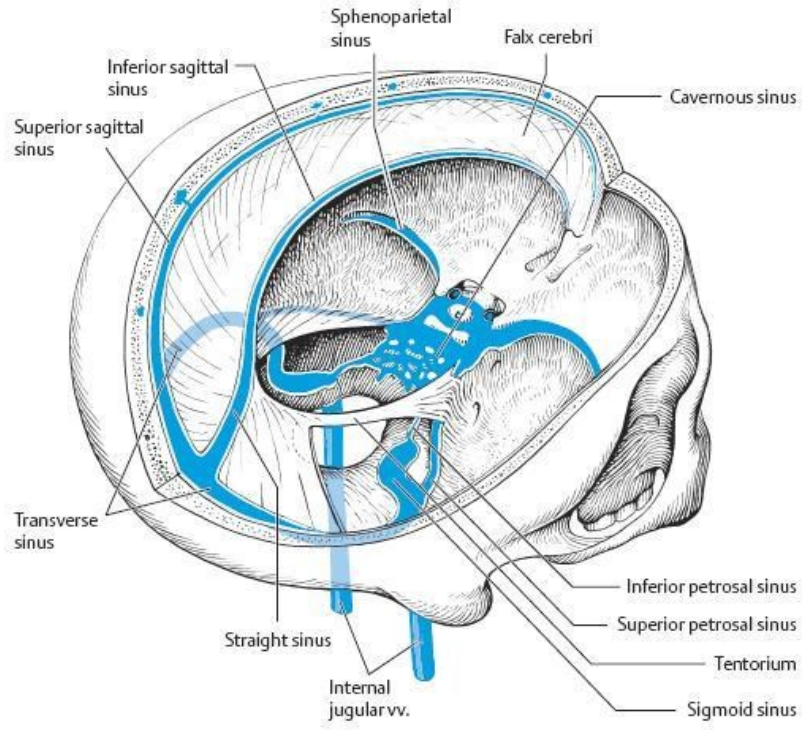

from Baehr M and Frotscher. Duus' Topical Diagnosis in Neurology. 4th ed Thime Stuttgart.New York. 2005; 238

Fig.2 Dural sinuses

1.2 Extracranial venous system

The main cerebral venous outflow tract in the neck consists of the *internal jugular vein (IJV)* and *vertebral venous system (Fig.3).* Venous flow from the superficial and deep venous system is toward the transverse sinus then the sigmoid sinus, which drains into the IJV. *The IJV* is joined by the subclavian vein to form the brachiocephalic vein. The confluence of the bilateral brachiocephalic vein is the superior vena cava (SVC), which ultimately drains venous blood into the heart (13). The existence of the IJV valve (IJVV) was initially described by Harvey (14). The IJVV is located about 0.5 cm above the union of the subclavian vein and the IJV at the lower limit of the jugular bulb (Fig. 2). IJVVs are seen in 96.8% of the general population. In the majority (93–99.1%) of subjects, the IJVV is bicuspid. The valve closes once during each cardiac cycle. The closure of the valve occurs during diastole when the contraction of right atrium while the tricuspid valve is open, transmits backward pressure from the right atrium into the SVC and then into the IJV. The valve is then open in mid-systole when the

pressure falls because the atrium empties into the ventricle following the opening of tricuspid valve (15). *Vertebral venous system* is a freely communicating, valveless system present throughout the entire spinal column and may be divided into an internal intraspinal part, the epidural veins, and an extraspinal paravertebral part. The vertebral venous system communicates with the deep thoracic and lumbar veins, intercostal veins as well as the hemiazygos and azygos veins. Abnormalities in these abdominal and thoracic veins may impair venous drainage from the vertebral venous system, which serves as an important collateral for cerebral venous drainage. The hemiazygos arch is connected with the left renal vein that represents a major outflow route for shunting blood into the inferior vena cava. Ultimately, the azygos vein serves as the final venous blood collector and drains into the superior vena cava. The vein is so named because it has no symmetrically equivalent vein on the left side of the body (13).

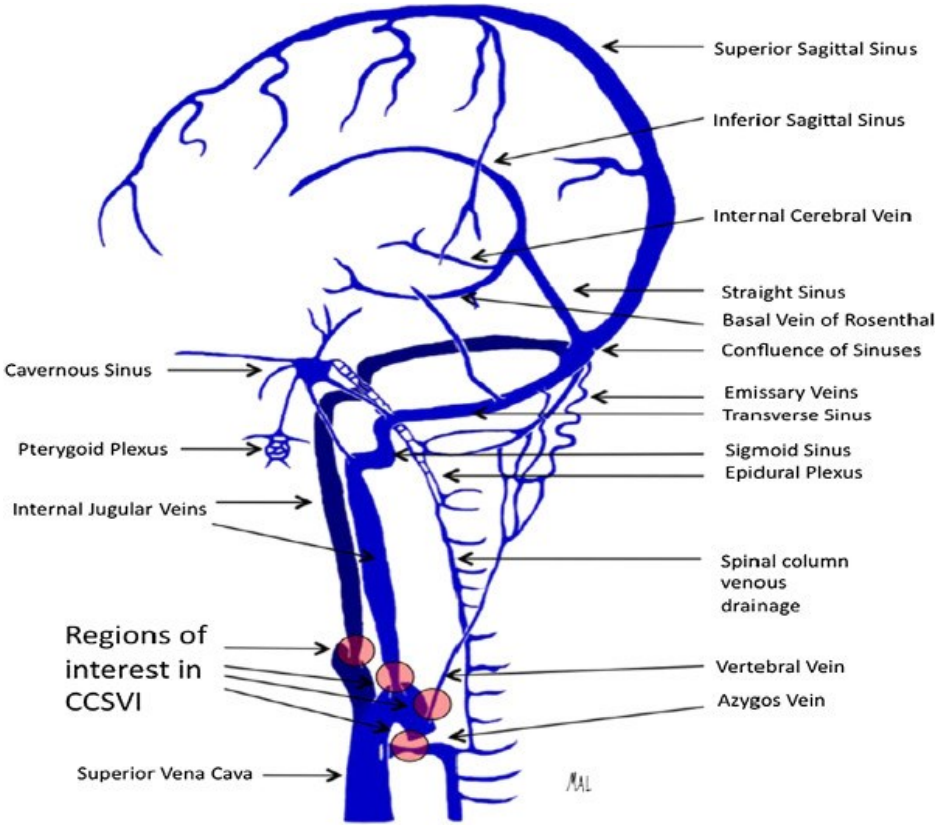

Fig.3 Extracranial venous system (from Zivadinov 2013 (13))

1.3 Physiology

Many factors and variables affect cerebral venous return. If these variables are kept constant, however, venous return (VR) is inversely proportional to the central venous pressure. Also, in hemodynamically stable conditions, VR is roughly equal to cardiac output.

CVS is influenced by the *thoracic aspiration*. At the time of expiration, the intrathoracic pressure is approximately -5 cm H_2O and forced inspiration generates even lower intrathoracic pressure of about -8 cm H_2O. The pressure gradient favors venous return to the right heart (4). The cerebral venous outflow depends mainly on *body position*, as demonstrated also by using a mathematical model by Gisolf (16). In supine position, IJVs are the main drainage routes for cerebral venous flow whereas in upright position, IJVs have negative intraluminal pressure, being located above the heart level, and therefore, they collapse. Therefore, in upright position, when IJVs collapse, the vertebral venous plexus, that is less efficient in supine position, represents the main alternative drainage route whose activation is position dependent (17). The *transmural venous pressure* of the spinal venous system is determined by the CSF pressure. The intracranial and spinal liquor system communicate freely by the foramen magnum. For this reason, the pressure gradient between CSF and veins is the forcing power of spinal venous blood flow. Under physiological conditions, there can be found in the horizontal position a pressure of 11 mm Hg at the level of craniocervical junction. In the upright position, CSF pressure at occipital niveau is subathmospheric (-5 cm H_2O) and, at lower spinal level, it can be reached a pressure of 40–45 cm H_2O (4).

Chapter 2

Vascular aspects of multiple sclerosis

2.1 Introduction

Multiple sclerosis (MS) is a disorder of the central nervous system (CNS) with autoimmune, inflammatory and neurodegenerative components which may influence each other or alternatively may have independent natural histories. Although the typical age of onset of MS is in the third and fourth decades of life, the burden of disease is most marked in the fifth to seventh decades (18). MS affects more than 2.5 million individuals worldwide (19), with higher incidence and prevalence in women than men (20). MS has a highly variable inter and intra-personal clinical course, both in pattern and rate of deterioration (18). In relation to aetiology, MS is a complex disease in which multiple environmental and lifestyle risk factors act together in a genetically susceptible individual to cause the disease (21). Environmental and lifestyle risk factors include low sunlight exposure and vitamin D, cigarette smoking and exposure to Epstein–Barr virus (20-23). In recent years, several studies have reported vascular abnormalities in patients with MS (24).

2.2 Vascular abnormalities

Three types of vascular dysfunction have been described in multiple sclerosis (MS). First, epidemiological data suggest that patients with MS might have an increased risk of developing ischaemic stroke. Second, imaging studies in patients with MS suggest a decrease in cerebral perfusion that affects widespread areas including the normal-appearing white matter (NAWM). Third, MS has been associated with reduced CNS venous blood drainage, which is referred to as chronic cerebrospinal venous insufficiency (CCSVI).

2.2.1 Multiple Sclerosis and ischaemic stroke

Two nationwide Danish studies have reported that patients with MS had about a 30% higher risk of dying from cardiovascular disease than the age-matched general population (25-26). Two large studies revealed more detailed information on the occurrence of cardiovascular disease in people with MS. The frequency of

hospital admissions for ischaemic stroke was higher among MS patients compared with patients without MS matched for age, sex, ethnic origin (age range 40-85 years) (27). In another a large population-based cohort study MS was associated with an increased risk of hospital admissions for ischaemic stroke that persisted during the entire 30-year-long follow-up period (28). Inflammation is widely accepted to play an integral part in the pathogenesis of atherosclerosis (29-30). Endothelial dysfunction is an early step towards overt atherosclerosis and the immune system seems to be highly involved in both processes (31). Alterations in endothelial function, as well as platelet activation and thrombophilia, have been reported in MS (32-33). Moreover, oxidative stress contributes to the development of endothelial dysfunction (34). The concentration of plasma homocysteine, which is believed to be an independent cardiovascular risk factor, is also raised in patients with MS (35-36). The cause of the increase in homocysteine concentration is unknown, but it occurs independently of serum concentrations of vitamin B12, vitamin B6, or folate (37). There is evidence that hyperhomocysteinaemia can cause endothelial dysfunction, even at moderately increased concentrations of homocysteine (38-39). The above evidence suggests that the increased frequency of ischaemic stroke in MS might be mediated through converging inflammatory pathways, oxidative stress, and raised homocysteine concentrations leading to endothelial dysfunction.

2.2.2 Cerebral hypoperfusion in Multiple Sclerosis

Cerebral perfusion is defined as the volume of blood flowing through a given volume of tissue per time unit. It consists of three parameters: cerebral blood flow (CBF), cerebral blood volume (CBV), and mean transit time. Single photon emission computed tomography and PET studies have shown that CBF is decreased in both the grey and white matter of patients with MS (40). Using dynamic susceptibility contrast-enhanced MRI (DSC-MRI), Law and colleagues (41) found markedly decreased CBF and prolonged mean transit time throughout the NAWM of the brain in 17 patients with relapsing-remitting MS compared with 17 control individuals. Adhya and colleagues (42) subsequently studied the regional pattern of perfusion in NAWM in 11 patients with relapsing-remitting MS, 11 patients with primary progressive MS, and 11 control individuals. They

concluded that both CBF and CBV were substantially decreased in all NAWM regions in patients with either form of MS compared with control individuals. Cerebral hypoperfusion in patients with MS might be secondary to axonal degeneration, leading to a decreased metabolic demand. Decreased axonal activity might reduce axonal K+ release and subsequent release in the perivascular spaces, possibly leading to a state of cerebral hypoperfusion. Energy metabolism of astrocytes seems to be dysfunctional in MS. Increased blood concentrations of the vasocostrictive compound endothelin-1 (ET-1) in patients with MS might also contribute to the widespread cerebral hypoperfusion (43-44).

2.2.3 Venous blood drainage in Multiple Sclerosis

Zamboni and colleagues (45-46) described an association between MS and a condition defined as CCSVI, which is characterized by a high incidence of reflux in both intracranial and extracranial venous segments, loss of postural venous outflow regulation, the presence of multiple stenoses of unknown origin in the internal jugular veins and azygos vein, and the opening of collateral circles.

They performed a specialized ultrasound protocol combining extracranial and transcranial Doppler (TCD) techniques, in a total of 65 MS patients and 235 control patients (45). Five specific parameters were evaluated and patients were considered to have an abnormal ultrasound, if any two of the five criteria were present, with 100% of MS patients and 0% of controls meeting those criteria.

The five parameters were:

1 - Reflux in the internal jugular veins (IJVs) and/or vertebral veins (VVs) in sitting and supine posture.

2 - Reflux in the intracranial veins. Reflux is defined as a reversal of flow direction during the inspiratory and expiratory phase during normal breathing with mouth closed.

3 - B-mode evidence of abnormalities in the IJVs, such as stenoses, malformed valve, annulus, septums, etc.

4 - Flow not Doppler-detectable in IJVs and/or VVs despite numerous deep breaths.

5 - Reverted postural control of the main cerebral venous outflow pathways, detected by measuring the difference in IJV cross-sectional area (CSA) between the supine and upright positions.

However, several other sonographic studies have been unable to replicate the findings of Zamboni and colleagues (47-50). Doepp and co-workers (47) did an extended ECD and TCDS study that included analyses of extracranial venous blood volume flow, cross-sectional areas, internal jugular vein flow during the Valsalva manoeuvre, and CCSVI criteria in 56 patients with MS and 20 control individuals. Except for one patient with MS, blood flow direction in the internal jugular veins and vertebral veins was normal, and none of the patients had internal jugular vein stenosis. Internal jugular vein and vertebral vein blood volume were equal in the supine position in both groups. No differences between the two groups were noted in intracranial veins or during the Valsalva manoeuvre. None of the patients investigated in this study fulfilled more than one criterion for CCSVI. Venous drainage via the internal jugular veins in the upright position was higher in patients with MS than in control individuals, which is an interesting but unexplained finding. Beggs (51) proposed that this difference in venous drainage might suggest that a greater proportion of venous blood from the brain flowed through the internal jugular veins because of stenoses in extrajugular venous pathways, but the Doepp team (47) replied that this was not the case. Mayer and colleagues (49) examined the extracranial and intracranial venous blood flow direction with colour-coded doppler sonography and the extracranial venous cross-sectional area of the internal jugular veins and vertebral veins in B-mode sonography to assess whether the five previously proposed CCSVI criteria were met in 20 patients with MS and 20 healthy control individuals. No participant had retrograde flow of extracranial or intracranial veins. Evidence of internal jugular vein stenosis was noted in 13 patients with MS and 16 control individuals. No patient with MS and one healthy control fulfilled at least two criteria for CCSVI. Both studies (47,49) were limited by the small sample sizes. The discrepancies between the positive and negative studies on CCSVI might be explained by methodological differences in examining venous CBF, which is technically more complex than the assessment of arterial blood flow.

A novel phase-contrast MRI technique that allows better visualisation of the cerebral veins was used by Sundström and colleagues (52) to investigate 21 patients with relapsing-remitting MS and 20 healthy control individuals. No differences were found between groups in internal jugular venous outflow, aqueductal CSF flow, or the presence of internal jugular venous reflux. At this present time, there are not sufficient conclusive evidence and there are reproducible differences on ultrasound between MS and control patients. Zamboni proposes that there is local, perivenular erythrocyte extravasation secondary to CCSVI, which results in iron overload and activation of the immune response (53).

Chapter 3

Cerebral venous system: Ultrasound techniques

3.1 Transcranial Doppler sonography

Transcranial Doppler sonography is a non-invasive, inexpensive, portable and safe technique that uses a pulsed Doppler transducer for assessment of intracerebral blood flow. The examination usually begins from the temporal window with an axial access, in mesencephalic plane and then goes on standardized planes according to the venous structure that needs to be studied. This approach allows to view the deep middle cerebral vein that is identifiable in correspondence of the passage between the M1 and M2 segments of the MCA. Its flow direction is away from the transducer. Pointing the probe downwards, through a slow inclination, it is possible to move, by means of a pontine plane, toward the bony structures of the middle cranial fossa, and then in the direction of the outflow region of the cavernous sinus. At the same time, it is possible to identify the sphenoparietal sinus, using as landmarks the edge of the small wing of the sphenoid bone and the medial head of the superior petrosal sinus, near the pyramid of the sphenoid bone, at the extreme medial edge of the petrous bone. Both sinuses present a flow direction that is away from the probe. On the other hand, tilting the probe in the opposite direction, from mesencephalic to diencephalic plane, it is possible to view the basal vein of Rosenthal. This vein has the same course as the posterior cerebral artery, both in the pre-peduncular segment, with the flow direction approaching the probe, and in the post-peduncular segment, with the flow direction away from the probe and with the course slightly more cranial compared to the posterior cerebral artery. Following the more distal part of the basal vein of Rosenthal, on the diencephalic plane, it is possible to view the vein of Galen, which is placed posteriorly to the hyperechoic signal of the pineal gland in the midline, with the flow direction away from the probe. With this scanning plane, the posterior head of the superior sagittal sinus can be simultaneously displayed, also with a direction away from the probe. The vein of Galen continues to the straight sinus, which runs along the insertion of the tentorium on the falx. Changing the scanning plane by tilting the probe postero-

superiorly and slightly rotating a few degrees in the direction of the internal occipital protuberance, the torcular Herophili or confluence of sinuses is reached. Also, the straight sinus has the flow direction away from the probe. Another venous structure that can be visualized by ultrasounds is the transverse sinus; it can be insonated through a contralateral and ipsilateral approach. The latter one helps to increase the rate of global insonation and to view besides the proximal segment also the medium and distal ones of the Transverse sinus, exploiting a more anterior window and using the bony landmark as a guide. The classic contralateral approach, when the torcular Herophili has been visualized, requires a lower tilting of the probe until the proximal segment of the transverse sinus, adherent to the skull bone, can be seen; the flow direction is away from the probe. The use of the occipital window is almost exclusively limited to the display of the inferior petrosal sinus, at the side of the basilar artery with flow direction toward to the probe. It is possible to view, although with lower rates of insonation, also the straight sinus, vein of Galen, and the internal cerebral vein (17).

3.2 Extracranial Doppler sonography

Subjects should be examined at least in sitting and supine positions. Either the IJVs and the VVs can be examined by using both the transversal and/or the longitudinal cervical access (54). The operator uses minimal pressure over the skin in order to prevent compressing the vein and thereby affecting the measurement, as previously reported (55-59). The operator can assess the following: flow direction, flow velocity, competence of the IJV valve, cross sectional area in relation to change in posture, and anomalous morphology. The flow direction, in either the IJVs or the VVs, can be measured during inspiration and/or expiration, but it is recommended to measure it in the respiratory pause (56). The direction of flow can be analyzed either with the pulsed wave sample placed in the vessel, at a 60° angle, or with the Colour Coded Mode, by comparing the colour of the flow in the IJVs/VVs with that of the satellite carotid and/or vertebral artery. According to consensus statements on peripheral vein ECD investigations, we define as monodirectional a flow always directed toward the heart. Flow is considered bidirectional when a flow reversal from its physiological direction for a duration < 0.5 sec. was detected. When the phase of

reverse flow is > 0.5 sec, it is defined as venous reflux (60-61). Assessment of Doppler flowmetry in ml/min by using the softwares included in the package of the ultrasound equipment, is performed at the level of the thyroid gland for the IJVs and at the level of C5-C6 for VVs (56). Therefore, it has been suggested to record flow measurement beginning two minutes after the change in posture and after several deep breaths in order to permit blood redistribution in the venous system. In the erect position, the vertebral venous system represents the major outflow pathway. Moreover, in the supine position, a duplex derived-flowmetry of 700±270 ml/m was measured in normal volunteers. This was found to change completely, however, when the subject changed to the upright position, as the IJV flow fell to 70±100 ml/m, whereas in the VV it rose from 40±20 to 210±120 ml/m (56). The apparent unexplained rest of about 450 ml/min in the standing posture represents the gravitational effect of the hydrostatic pressure, which causes the displacement of 70% of the total volume of blood below the heart level (62). From this point of view, the higher hydrostatic column in the valveless vertebral-azygos system in the erect position favours venous drainage through this route, rather than through the IJV. It has been reported that it is possible to observe IJVs stenosis and, in contrast, also IJVs aneurysms. An asymmetry, defined as a cross sectional area (CSA) at least twice that of the contralateral IJV was noted in 62.5% of cases. In addition, stenosis of the IJVs with a CSA of 0.4 cm^2 or less was measured in 23% of cases (63). ΔCSA in the IJVs, obtained by subtracting the CSA measured in the supine from that in the sitting position, is a positive value in normal subjects (4,55, 56, 57). In fact, CSA variation reflects the variation of blood volume which flows in the IJV in response to changes in hydrostatic pressure determined by the different bodily positions (64-65).

3.3 Ultrasound contrast agents

Contrast–enhanced US is an noninvasive imaging tool for the assessment of microcirculation that is able to help identify, in vivo, disturbed regulatory events at the capillary and postcapillary level. US contrast agents are true intravascular agents that, unlike the diffusible agents commonly used in MR imaging and CT, remain entirely within the vascular space and possess intravascular rheological characteristics similar to those of red blood cells. On the basis of the assumption

that the time required by the US contrast agent to pass from the cerebral arteries to the veins should be prolonged in presence of small-vessel disorders, contrast-enhanced US with intensity curve analysis can be used to evaluate tissue perfusion. To date, two substances have been approved for non-cardiac human use in Europe. The first, Levovist R (Schering, Berlin, Germany), consists of air bubbles generated by adsorption of galactose particles in an aqueous solution and stabilized by a palmitate layer. The other, SonoVue R (Bracco-Altana, Konstanz, Germany), consists of sulfur hexafluoride, which forms microbubbles, stabilized by a phospholipid layer, once dissolved in water. Besides their approved use in the liver, where they improve the detection and characterization of focal lesions, contrast ultrasound agents may assist in the assessment of blood flow in tissue, and thereby of tumor viability and perhaps tumor aggressiveness. When an ultrasound pulse hits a microbubble it will resonate at a frequency mainly determined by its diameter. It is a lucky coincidence that this resonance frequency is in the range between 2 and 5 MHz and thereby matches the spectrum of most abdominal ultrasound transducers. Looking closer, however, the reflected signal will not entirely mirror the transmitted pulse, since the oscillations of the microbubbles are asymmetrical. In simple terms, the expansion will be more pronounced than the contraction. When the reflected signal is analyzed in the frequency domain it will therefore, in addition to the fundamental (transmitted) frequency, contain higher-frequency components, i.e. harmonics. This behavior of microbubbles—concerning both upper and lower harmonics and the fundamental frequency—is referred to as ‘nonlinear backscattering’. At higher power of the transmitted signal the bubbles will rupture, following a short series of expansion and collapse. As the bubbles perish they emit a final, short-lasting signal, a stimulated acoustical emission (SAE) (66).

Chapter 4

Experimental studies

4.1 Internal Jugular Vein Blood Flow in Multiple Sclerosis Patients and Matched Controls.

4.1.1 Introduction

Compared with the cerebral arterial system, the cerebral venous system has been less well described and studied and this might lead to an underestimation of cerebral venous disorders. Unlike the carotid artery, the vascular wall of the IJV is much more flexible with a variable lumen diameter and this makes more difficult to perform a quantitative study of blood flow. The internal jugular veins (IJVs) are the main pathway for venous outflow in the supine position, while in the upright posture the IJVs collapse and venous outflow occurs mainly through secondary veins such as the vertebral, epidural, and deep cervical veins, which compose the vertebral venous plexus (4,56). The hemodynamic of the IJVs may reflect cerebral venous drainage conditions and appear to influence intracranial hemodynamic, perfusion of the brain and the dynamics of Cerebrospinal fluid system (67). The insufficient cerebral venous drainage could cause a variety of unspecific central nervous symptoms such as headaches, visual disturbances, or amnestic dysfunctions (68). Several studies have found a relationship between IJV drainage abnormalities and certain neurological diseases of undetermined aetiology (69-70) including leukoaraiosis (71) dementia (72) and normal-pressure hydrocephalus (67) and, recently, MS (45,73). The dependence of enhancement by time can be shown in a timeintensity curve (TIC) where the average signal from a Region of Interest (ROI) is plotted as a function of time. The integration of modern ultrasonographic equipment with dedicated signal-processing systems overcomes the operator-dependent analysis of the ultrasonic signal. From a TIC can be obtained some temporal and amplitude parameters, such as tissue and vascular uptake, transit times, and wash-out of the contrast agent.

The present study describes a new and simple approach to cerebral venous analysis, based on the use of ultrasound contrast agent imaging with time intensity curve analysis (74).

4.1.2 Material and Methods

All subjects voluntarily participated the study after written informed consent concerning treatment of personal data, background and objective of the study, methodologies and duration of ultrasound assessment. “Carlo Romano” ethics committee of the Federico II University of Naples approved this no-profit study.

Subjects. This study included 58 consecutive patients affected by clinically defined MS diagnosed according to the revised McDonald criteria, 7 patients with Clinically Isolated Syndrome (CIS), and 13 age- and sex-matched healthy controls.

Inclusion criteria for patients with MS were as follows:

- age 18–60 years
- EDSS between 0 and 6.5.

Exclusion criteria were as follows:

- presence of relapse
- steroid treatment in the 30 days preceding study entry for all patients
- pregnancy
- preexisting medical conditions known to be associated with brain pathology

All of the participants underwent a clinical examination and extracranial duplex sonography of the neck in the same week.

Disability was graded by using Kurtzke’s Expanded Disability Status Scale (EDSS) and Multiple Sclerosis Severity Score (MSSS). Electrocardiography was performed and fasting venous blood sample was drawn for routine laboratory examination including blood clotting and screening for thrombophilic status.

Ultrasound studies. All patients with MS and control subjects underwent extracranial color Doppler evaluation. This ultrasound examination was performed by the same radiologist with the iU22 Ultrasound System (Bothell WA, U.S.A.) equipped with a 9–3 MHz, linear-array probe. The cross-sectional area of

the internal jugular vein (IJV) was measured in the horizontal plane at the level of the thyroid gland, perpendicular to the vessels. Extracranial duplex US was performed in all subjects to exclude carotid artery and /or IJV stenosis. For contrast-enhanced US, a bolus of 2.4 mL of an echo-contrast enhancer (sulfur hexafluoride, SonoVue; Bracco, Milan, Italy) was manually injected into the left antecubital vein after a 10-minute resting time in the supine position, followed immediately by a 10-mL saline solution bolus, and a 1 minute B-mode cine loop was acquired. Then, after 10 minutes, a second intravenous bolus of 2.4 mL of SonoVue was repeated for the evaluation of contralateral side. Electrocardiography was used to monitor the heart rate during the test. An area of the neck where the IJV and thyroid gland appeared in the same transverse plane was located by using color Doppler and designated for analysis. The wash-out curve was analyzed offline in a blinded way, by using a time-signal intensity curve analysis program QLab (Philips Healthcare) that displayed the acoustic intensity (in decibels) during the acquisition time in a manually defined region of interest. To reduce the artifacts caused by peak intensity variations, contrast agent arrival was defined as the time point of a stable signal intensity enhancement of at least 5 dB in the IJV. Nine semiquantitative perfusion parameters were extracted from the time-intensity curves in the ROI designated for analysis at level of Internal Jugular Vein (IJV):

1) Arrival time was defined as the time from injection of contrast agent to the beginning of signal intensity increase;

2) Absolute Intensity Peak (dB) was the maximum intensity at the peak of the intensity curve;

3) Time to peak intensity (in seconds) was defined as the time from injection of contrast agent to reach the peak of contrast intensity;

4) Incremental Time (in seconds) was calculated as the difference between time to peak intensity and arrival time;

5) Enhancement slope (dB/s) was calculated as the ratio between intensity peak and incremental time

6) Area under the curve (AUC) during wash-in (dB x sec) was calculated from the point of the increase in image intensity greater than 5 dB above the baseline to the peak intensity;

7) AUC during washout (dBs) was calculated from the peak intensity to the end of 1 minute acquisition;

8) minute residue value (averaged contrast enhancement values at 58 to 60 seconds);

9) minute wash-out rate (calculated according to the following equation: 1-minute wash-out rate = (peak enhancement value – 1-minute residue value)/peak enhancement value x 100.

IJV valve incompetence with retrograde flow was considered to be present when microbubbles appeared at B-mode imaging in the IJV before they appeared in the carotid artery. The time-dependent signal intensity changes of imaged area was classified into one of six predefined TIC shape categories, which is associated with a color (Fig 4).

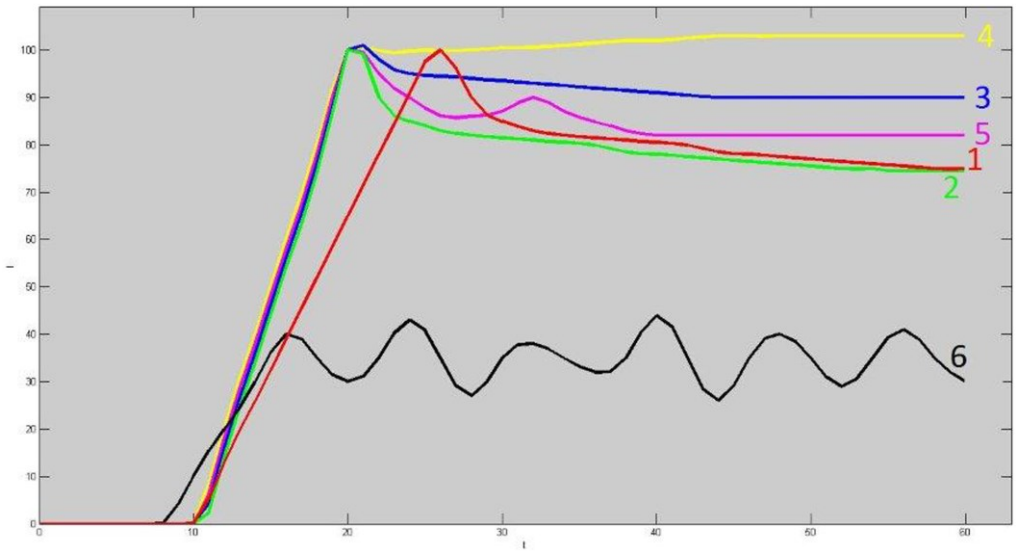

Figure 4. Graph of six time-intensity curves shape types (TIC). Type 1 shows slow enhancement followed by wash out phase; type 2 fast enhancement followed by wash out phase; type 3 fast enhancement followed by plateau phase; type 4 fast enhancement followed by gradual enhancement increase; type 5 fast enhancement followed by a short time wash out and by a second peak of enhancement; type 6 unclassified enhancement. Type 1–2 TIC shapes were considered indicative of fast wash-out. Type 3-4-5 were considered indicative of a slow venous wash-out. (from Mancini 2014 (74))

A curve was generated for every participant and the distribution of the different TIC shapes throughout the IJV was described (Fig.1). We also assessed the left and right prominence of the other most important veins in the neck visible on CEUS imaging of the neck: external jugular veins, anterior jugular veins, facial veins, thyroid veins, and deep cervical veins. The number of collateral veins for the right and left side of the neck was counted.

Statistical Analysis. Statistical analyses were performed using SPSS (version 18.0 Chicago, IL). Continuous data were reported as median and range, and categorical data were reported as percentages. An unpaired nonparametric test (the Mann-Whitney U test) was used for comparison of contrast enhanced US parameters between the MS and control groups. Kruskal-Wallis analysis of variance was used to compare more than two groups. The post-hoc analysis was performed by means of the Dunn test. Fisher's exact test, and the χ^2 test were used to determine differences between categories. The Spearman's rank correlation (ρ_s) coefficient was used to verify if variables were associated. Residual analysis was performed to assess differences in the distribution of venous criteria among MS subtypes. Significance was denoted when p was < 0.05 by using two-tailed tests.

4.1.3 Results

Demographic and clinical characteristics of MS patients, CIS, and control groups are shown in Table 1.

Table 1. Demographic and clinical characteristics of HCs, CIS patients, all MS patients and MS subtypes patients.

	HCs	CIS	MS Patients					
					MS Subtypes			
			Whole Group	p§	RR	SP	PP	p*
No.of Subjects	13	7	58		32	20	6	
M	9	3	13		7	2	4	
F	4	4	45	0.089	25	18	2	
Age (y)	35	33	41	0.002	35	43	49	0.001
	(23–54)	(27–41)	(25–60)		(25–54)	(27–55)	(35–60)	
Onset age(y)		27	29	0.336	26	31	36	0.061
		(24–41)	(8–47)		(8–37)	(19–37)	(22–47)	
Disease duration (y)		1	4	<0,001	8	11	15	0.002
		(0–7)	(2–7)		(1–31)	(2–30)	(6–18)	
EDSS		2	4.2	<0,001	3.5	4.5	6	<0,001
		(1,5–3,5)	(2–6,5)		(2,0–4,5)	(3,0–6,0)	(4,5–6,5)	
MSSS		2	1.78	<0,001	3.5	4.5	5.5	<0,001
		(1,5–3,5)	(0,13–12,76)		(2,0–4,5)	(4,0–6,0)	(4,5–6,5)	

Data are expressed as median and range (in brackets). There were no statistically significant differences between HCs and MS patients in age (p = 0.721; 0.153) or sex (p = 0.148; 0.332). § Mann-Whitney *U* test between CIS and MS patients. * Kruskal Wallis one-way analysis of variance among MS patients.
HCs = healthy controls subjects; CIS = clinically isolated syndrome; MS = multiple sclerosis; MS Subtypes: RR = relapse remitting; SP = secondary progressive, PP = primary progressive.
doi:10.1371/journal.pone.0092730.t001

(from Mancini 2014 (74))

Significant differences in age, EDSS, MSSS and disease duration were evident in the subgroups. Patients with MS patients had different clinical forms of the disease (32 RR MS, 20 SP MS and 6 PP MS). Thirty-two (55%) of 58 patients with MS were receiving disease modifying therapies (interferon beta-1, natalizumab, glatiramer acetate, fingolimod, azathioprine, and mitoxantrone).The contrast agent was well tolerated in all individuals, without substantial side effects. Internal jugular vein reflux was observed in 14 veins. Internal jugular vein wash-out rate and wash-out AUC were significantly increased in patients with MS compared with CIS and HCs (Table 2).

Table 2. Parameters of time intensity curve in Healthy Controls (HCs). CIS and patients with MS.

	HCs	CIS	MS patients					
					MS Subtypes			
			Whole group	*p*	RR	SP	PP	*p* *
IJV CSA supine (cm^2)	0.8	0.4	0.8	*0.207*	0.7	0.8	1.2	*0.184*
	(0.4–2.1)	(0.3–1.3)	(0.1–3.4)		(0.1–2.2)	(0.1–3.4)	(0.1–2.3)	
Wash–in parameters								
Intensity Peak (dB)	81.2	83.2	91.0	*0.040*	88.6	92.7	102.6	*0.135*
	(4.9–99.6)	(53.0–121.5)	(5.9–122.7)		(5.9–122.7)	(7–121.9)	(10.5–119.7)	
Incremental Time (s)	9.0	9.5	10.1	*0.115*	10.1	10.0	10.4	*0.341*
	(6.9–14.1)	(5.9–12.9)	(4.9–27.9)		(5.1–27.9)	(4.9–18.3)	(5.5–17.1)	
Enhancement Slope (dB/s)	8.7	10.1	8.6	*0.534*	8.8	8.0	8.7	*0.784*
	(0.7–12.6)	(5.1–15.9)	(0.6–21.0)		(0.6–18.5)	(1.4–13.7)	(1.7–21.0)	
Time to Peak intensity (s)	23.3	22.0	23.2	*0.257*	23.2	22.6	26.0	*0.326*
	(18.1–33.4)	(16.2–26.2)	(6.5–38.0)		(14.8–38.0)	(6.5–36.6)	(18.4–33.6)	
AUC wash in (dBs)	346	442	505	*0.013*	501.5	527.8	741	*0.046*
	(14–715)	(260–705)	(19–1725)		(29–1725)	(19–1166)	(26–957)	
Wash-out parameters								
Residual value (dB)	53.9	57.2	70.4	*0.009*	66.8	72.0	85.5	*0.035*
	(1.5–72.1)	(34.8–98.4)	(70.4–114.2)		(3.7–114.2)	(4.3–101.3)	(4.3–105.0)	
Wash-out rate (%)	33.4	30.0	22.2	*0.003*	22.9	23.5	16.0	*0.014*
	(16.2–76.8)	(8.1–43.0)	(2.7–65.9)		(2.7–65.9)	(5.7–57.1)	(10.4–64.1)	
Lower value	28.3	21.6	17.1	*0.014*	18.2	18.2	14.5	*0.036*
	(16.2–45.1)	(8.6–36.1)	(2.7–49.5)		(2.7–49.5)	(5.7–46.8)	(10.4–24.5)	
AUC wash-out (dBs)	2 241	2 617	2 701	*0.023*	2 701	2 630	3 136	*0.098*
	(78–3 010)	(1 437–4 167)	(109–4 537)		(109–4 537)	(266–4 424)	(246–3 938)	

* Kruskal-Wallis analysis of variance.
All results are expressed for veins only the lower wash-out rate was evaluated for patients and calculated as the lowest value between the IJV for each patient.
doi:10.1371/journal.pone.0092730.t002

(from Mancini 2014 (74))

Even after jugular veins with retrograde flow were excluded from the statistical analysis, washout rate values remained significantly lower in the MS group compared to HCs and CIS [in MS patients without retrograde flow WO rate was 24.7% (range, 2.7–64.1%) CIS 29.2% (range, 13.3–42.9%) and HCs 35.4% (range, 16.2–76.8%) $p<0.05$]. No significant differences were found between the MS, CIS and HCs in all wash-in parameters excluding intensity peak and AUC wash in (Table 3).

Table 3. Cross-correlation matrix coefficients.

	Age (y)	Age at onset (y)	disease duration (y)	EDSS	MSSS	total relapses (n)	relapses in the last 2 years
IJV CSA (cm^2)	0.215	0.155	0.195	0.089	0.300*	−0.061	0.105
Wash-in parameters							
Intensity Peak (dB)	0.129	0.238	−0.117	0.054	−0.069	0.207	−0.125
Incremental Time (s)	0.185	0.099	0.156	0.025	−0.089	−0.251	0.055
Enhancement Slope (dB/s)	−0.027	0.187	0.256*	−0.074	−0.115	0.247	−0.160
Time to Peak intensity (s)	0.286*	0.302*	0.124	0.012	0.032	−0.177	0.194
AUC wash in (dBs)	0.126	0.139	0.085	0.161	−0.061	0.025	−0.085
Wash-out parameters							
Wash-out rate (%)	−0.067	−0.204	−0.005	−0.038	0.044	−0.137	0.065
Lower value	−0.135	−0.346*	−0.082	−0.402*	−0.252	−0.120	0.024
AUC wash-out (dBs)	−0.019	0.179	−0.135	0.066	−0.118	0.222	−0.132

The numbers represents the Spearman's rank correlation coefficient value. * p<0.05.
doi:10.1371/journal.pone.0092730.t003

(from Mancini 2014 (74))

The right jugular vein was significantly larger than left jugular vein (CSA in right IJV 0.83 cm^2 vs. left IJV 0.67 cm^2 p = 0.028) and showed lower WO rate [WO rate right 19.7% (2.74–53.44%) left 24.9% (5.32–65.86%)] and higher intensity peak [right 91.2 dB (5.88–122.68) left 87.13 dB (6.69–121.9)]. All washout time parameters were similar in male and female patients with MS. No difference was found between treated and untreated patients with MS (p = 0.857). There was a significant association between age at onset, increased EDSS and decreased WO rate in MS patients (table 3) calculated for each patient as the lowest value between the two IJV that is the value that takes into account for each patient the more diseased vein (age at onset r = - 0.346 EDSS r = - 0.402, $p < 0.05$, Table 3). The time- intensity curve (TIC pattern) of the HCs consisted predominantly type 2 fast WO (fast wash-in enhancement followed by fast WO phase) and was observed in 73% of HCs in 16% of MS patients. The TIC pattern predominantly in MS patient was type 3 [fast wash-in enhancement followed by delayed WO (46.4% of MS patients and 8.3% of HCs; $p < 0.001$)] (Figure 5).

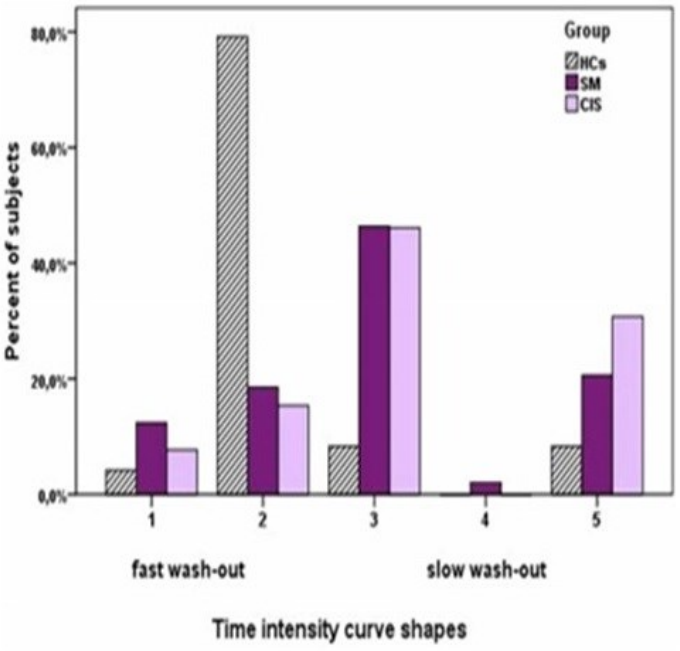

Figure 5. Frequency of Time intensity curve shapes in the different groups of subjects. The curve shapes 1-2 corresponds to a fast wash-out. The curve shapes 3-5 corresponds to slow wash-out. (from Mancini 2014 (74))

Subjects with higher number of collateral veins (> 2 collaterals) showed higher IJV intensity peak [82.3 dB (4.8–122.6) vs. 91.0 dB (5.9–122.7) p = 0.044]. A non-significant trend to higher residual value and AUC WO [residual value 59.2 dB (1.5–109.2) vs. 72.3 dB (3.7–114.2) p = 0.07; AUC WO (2 429 (78–4 464) vs. 2 757 (109–4 537) p = 0.083] was observed in MS patients with higher number of collaterals.

4.1.4 Discussion

We utilized CEUS to describe and quantify the IJV outflow in MS, CIS and HC. The main result was that MS patients showed, on average, approximately 30% reduction of the venous outflow through the IJV in supine position measured as WO rate percentage. The WO rate was reduced more in patients with primary progressive MS than in patients with RR MS or CIS. These findings suggest than the altered IJV dynamics could be a consequence rather than a cause of MS.

One common feature of CCSVI is stenosis of one or both IJV with a greater cerebral venous outflow resistance (75) that could reduce the flow rate of the ultrasound contrast agent through the IJV.

Our results are comparable to the studies that utilize quantitative methodology to evaluate alteration of cerebral venous drainage (76-77). The IJV wash-out rate could represent a more comprehensive quantitative measure of the severity of drainage impairment and, therefore, may be more useful in predicting clinical outcome than other imaging modalities that outcome categorical diagnosis. The slope enhancement, peak intensity, and time to peak values are similar in MS and HCs and indicates that total amount of contrast agent passing through the ROI is similar in MS and HC and that venous filling with blood coming from the brain occurs with normal velocity. Therefore, the differences in the time courses (expressed as higher plateau of the wash-out phase) indicate an obstructive pattern with slower drainage of the vein, reduction of outflow and accumulation of contrast in the vessel. Time Intensity Curve reflects the inflow and outflow venous dynamics represents venous physiology and could be associated with venous patency or obstruction. Using TIC shape analysis in our study, it was possible to demonstrate a significant difference between patients with MS and HCs. The TIC shapes differed significantly in the two groups. The type 2 TIC shape consists of a rapid enhancement phase followed by an early washout is the more frequently observed in healthy controls and is the normal IJV dynamics. TIC shapes with initial rapid enhancement followed by a plateau phase or gradual increase of the enhancement, or by a second peak of enhancement were associated with MS.

One hypothesis is that alteration of IJV outflow might be secondary to reduction of driving force of thoracic pump due to a weak respiratory muscular contraction of the chest (78) occurring early in the disease course and gradually worsening over time or secondary to some medications, such as muscle relaxants, that can depress breathing.

However all these conditions have been ruled out in patients in this study who were almost all young and without other cardiac or systemic diseases associated with Multiple Sclerosis. Moreover, compression of the veins draining the central

nervous system by a muscle can be another cause of compromised cerebral venous outflow. The omohyoid muscle is usually located next to the IJV and it is known that an atypical omohyoid muscle can compress the IJV and in this way may affect cerebral venous drainage (79). Recently Dolic et al., using MR venography, found that 22% of MS patients present with extraluminal abnormalities of the IJVs (80). Jayaraman et al., who evaluated these veins using CT angiography (81), found a similar prevalence of severe extrinsic stenosis of the IJVs. A limit of the study is the low number of the control group due to ethical limitations to the use of contrast agent in normal subjects without any clinical indications. A general limitation of quantifying replenishment kinetics is the dependence on the microbubble destruction and detection that could cause more complex replenishment kinetics.

4.2 Head and Neck Veins of the Mouse

4.2.1 Introduction

The majority of the studies on mouse cerebral vasculature focused on the arteries and no study of the venous system has been reported. Due to the high complexity of the cerebral vasculature and the difficulty in obtaining high resolution in vivo imaging of cerebral mice vessels, the study of this anatomy is a challenging task. The aim of the present study was to characterize the anatomy of the venous outflow of the mouse brain using different imaging techniques (82). As a reference work, the mouse cerebrovascular atlas by Dorr et al. (83) was used.

4.2.2 Material and Methods

Ten C57/black male mice (age range: 7-8 weeks) were imaged with high frequency Ultrasound, Magnetic Resonance Angiography and ex-vivo Microcomputed tomography of the head and neck. All procedures were approved by the local ethical committee.

High Frequency Ultrasound with Color Doppler. Under general anesthesia, color flow Doppler sonography was performed to provide a general overview of the neck veins. Before ultrasound examination, hairs were removed from the neck

and thorax with a depilatory cream to obtain a direct contact of the ultrasound gel to the skin of the animal minimizing ultrasound attenuation. To provide a coupling medium for the transducer warm gel was used. An outer ring of thick gel (Aquasonic 100; Parker Laboratories, Orange, NJ) was filled with a thinner gel (echo Gel 100; Eco-Med Pharmaceutical, Mississauga, Ontario, Canada) over the region of interest. Precise and repeatable control over the position of the two-dimensional image plane was obtained with a rail system (Vevo Integrated Rail System II; Visualsonics, Canada). High Frequency Ultrasound was performed with Vevo 2100 (Visualsonics, Canada) and a 20 MHz MicroScan transducer (MS250; Visualsonics, Canada) was used (bandwidth 13–24 MHz, axial resolution 75 μm, lateral resolution 165 μm, color Doppler frequency 16 or 21MHz, Pulsed Doppler frequency 16 MHz, minimum sample volume 0.19 mm). The veins were tracked in the anterior segment of the neck, the blood velocity was determined positioning the cursor placement depth at center of the vessel, the Doppler angle of insonation was maintained below 60°, and samples size was always kept as small as possible. Five readings were averaged, for the pulsatile waveform the lower velocity (EDV) the mean and peak velocity (PSV) and pulsatility index were measured (PI = systolic diastolic/mean).

Magnetic Resonance Angiography. Magnetic Resonance data were collected on 9.4 T or 7 T Bruker Biospec (Ettlingen, Germany) scanners with a volume transmitter coil and a four-channel rat brain receiver coil. For a global coverage of the whole brain and neck, time-of-flight (TOF) Magnetic Resonance Angiography (MRA) was performed using two multi-slice 2D axial spoiled gradient echo (FLASH) sequences acquired with a flip angle of 80°, a repetition time of 11.8 ms (9.4T) or 19.14ms (7T) and an echo time of 3.9 ms (9.4T) or 4.68 ms (7T) and 8 averages. A field-of-view of 20x20x18.7 mm^3 has been acquired with an in-plane resolution of 52 μm (pixel bandwidth: 233 Hz) and 85 slices of 300 μm thickness (slice overlap: 27%). Each MRA sequence was repeated twice, once with a saturation band positioned at a the thoracic outlet level to null the signal coming from protons in the arterial vessels, and once without the band, thereby displaying the flow signal from both arteries and veins of the head and neck district.

Micro silicon-CT imaging. Ex vivo micro-CT vessels imaging requires the filling of vessels with a radiopaque compound. An inert silicone rubber compound (MICROFIL, FlowTech Inc., MA) with a low viscosity was perfused in mice to have a complete filling of the cerebral and neck vasculature (84-85). In anesthetized mice, an incision was done through the midline of the sternum and the heart was exposed. A 24-gauge IV catheter was connected to a digital peristaltic pump (Peri-Star Pro, 2 channel, High rate, large tubing 220V, WPI Word Precision Instruments, Inc.) and inserted into the left ventricle of the heart and a cut over the right atrium is done. Through an incision on the right atrium the blood in vessels was drained out and then replaced by warm heparinized (5 U/mL) phosphate buffered saline for 5 minutes. The Microfil (1:2 mixture of Microfil to diluent and 5% (v/v) curring agent) was perfused for about 2 min to allow the Microfil to circulate through the cerebral vascular system and was allowed to cure at room temperature for 90 minutes. Microcomputed tomography (Micro-CT) was performed with the scanner Explore Locus (GE Healthcare, Manchester, UK) using the following parameters: 80K X-ray tube voltage, 450 μA X-ray tube current, scan technique 360°. A 160 minutes scan with a spatial resolution of 27 μm was performed. After reconstruction, images were calibrated in Hounsfield units (HU). Qualitative analysis was performed to obtain a tridimensional representation of the cerebral and neck vasculature (86).

4.2.3 Results

The study of cerebral outflow showed a number of large veins and sinuses. The cerebral venous outflow of the mouse consists of three paired extracranial districts:

- external jugular veins (EJVs),
- internal jugular veins (IJVs)
- vertebral veins (VVs).

Intracranially, the most anterior vein visible was a single, median straight vessel, that may be termed the “olfactory sinus”, as it courses dorsally in the olfactory sulcus. After a short rectilinear course, it joins the rostral rhinal veins that form a ring around the olfactory bulbs (Fig 6). These veins originate at the dorsal margin of the olfactory bulbs, extend forward, turn and run inferiorly following the border

between the olfactory bulbs and the frontal lobes. These veins drain into the anterior portion of the superior sagittal sinus (SSS) and connect laterally with the superficial temporal vein that begins superficially at the medial corner of the eye as the angular vein and supraorbital vein (Fig 7).

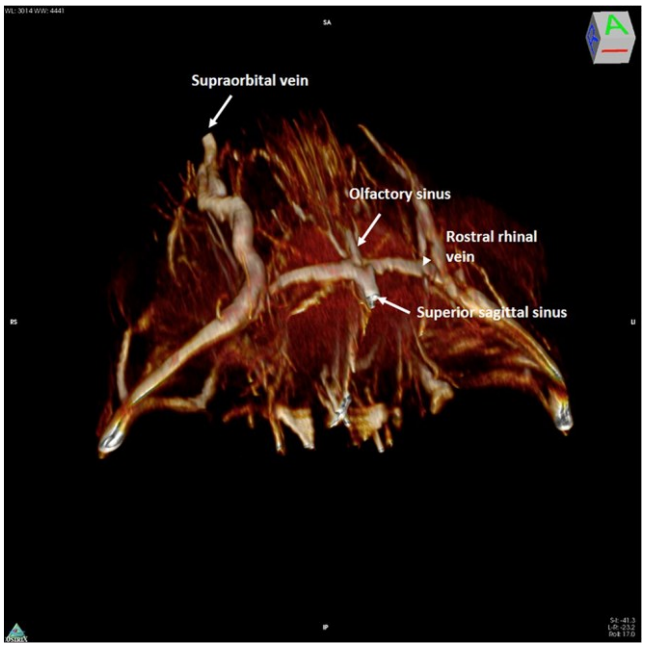

Fig 6. 3D rendering of magnetic resonance angiography acquisition of the rostral part of the mouse head. The mouse head is seen from above (the back of the head has been removed in post-processing). The anterior confluence of the median olfactory sinus (thin arrow) with the paired rostral rhinal veins (arrowhead) and the beginning of the superior sagittal sinus (thick arrow) is shown. Extracranially the supraorbital vein is visible. (from Mancini 2015 (82))

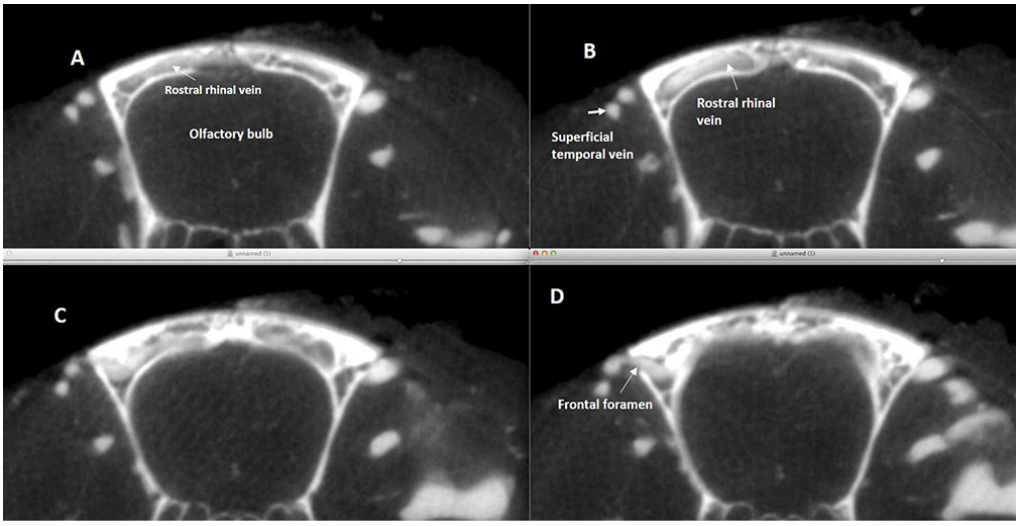

Fig 7. Axial silicon-microcomputed tomography of the rostral rhinal vein. (A-D) Four consecutive axial silicon- microcomputed tomography slices in cranio-caudal sequence showing the drainage of each rostral rhinal vein, which, after an intraosseus course, joins with the ipsilateral superficial temporal vein, through the frontal foramen. (from Mancini 2015 (82))

The caudal rhinal veins lie in the lateral section of the temporal–parietal lobe and occipital lobes, draining the lateral aspect of these cortices. Posteriorly, the veins join the Transverse sinus (TS), where the occipital lobe meets the cerebellum (Fig 8).

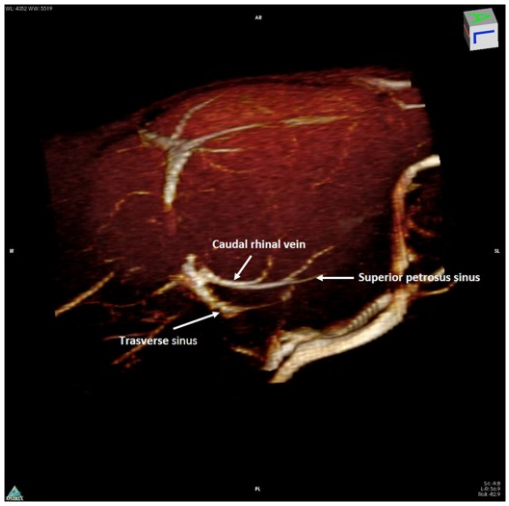

Fig 8. 3D rendering of magnetic resonance angiography acquisition of the mouse head. 3D rendering of magnetic resonance angiography acquisition of the caudal part of the mouse head, as seen laterally from a postero-superior angle. The confluence of the left caudal rhinal vein with the ipsilateral transverse sinus, as well as the junction of the superior petrosus sinus, are shown. (from Mancini 2015 (82))

The SSS starts anteriorly (Fig 9) and drains the dorsal and lateral parts of the frontal and parietal areas. The vessel originates behind the junction of the olfactory bulb and the frontal lobe, courses along the curvature of the inner table of the skull, in the interhemispheric sulcus, to reach the confluence of sinuses. In its course, the sinus is interconnected supraorbitally with the rostral rhinal veins, branches of superficial temporal vein and facial vein, and receives venous tributaries of the superficial venous system (anterior superficial cerebral vein). The SSS drains into the confluence sinuum together with the straight sinus (Figs 10, 11A and 11B). Veins that lead directly into this confluence drain a portion of the occipital cortex (Fig 12).

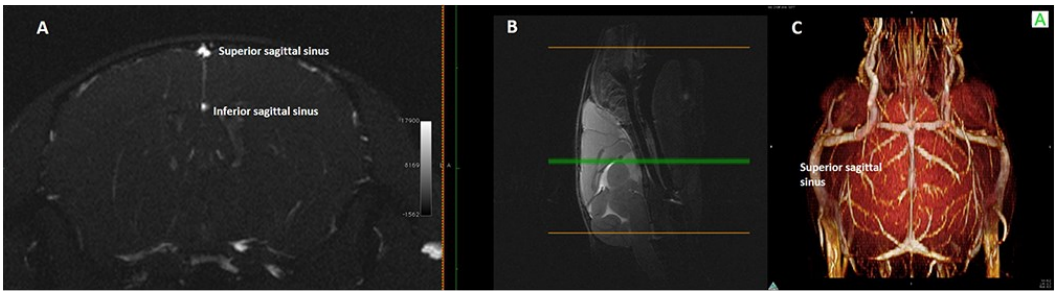

Fig 9. Single axial magnetic resonance angiography partition and 3D rendering of mouse head. (A) Single axial magnetic resonance angiography partition at the mid-level of the brain hemispheres ((B) midsagittal T2w slice used as a reference) and (C) 3D rendering of magnetic resonance angiography acquisition of a mouse head, as seen from above, the position of the superior sagittal sinus and inferior sagittal sinus is clearly shown as well as the connections of the former on the dorsal surface of the brain. (from Mancini 2015 (82))

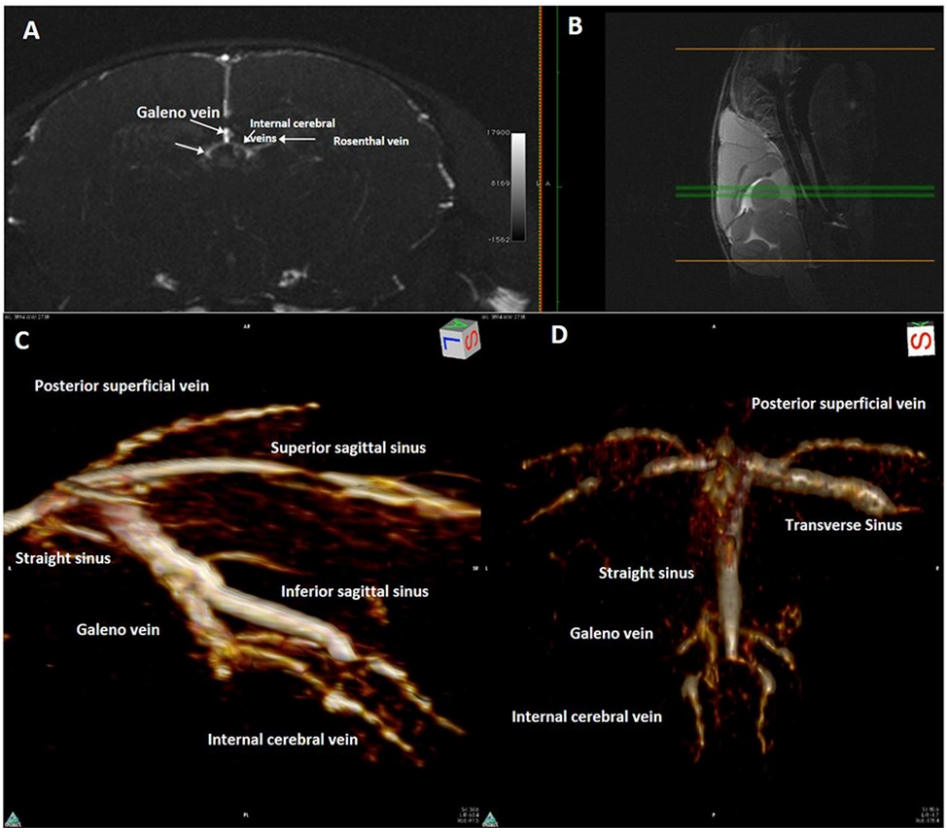

Fig 10. Magnetic resonance angiography and 3D of the caudal part of confluence of sinuses, and the deep brain venous system. (A) Maximum Intensity Projection of axial magnetic resonance angiography partitions at the mid-level of the brain hemispheres ((B) mid-sagittal T2w slice used as a reference,) and 3D rendering of magnetic resonance angiography acquisition of the caudal part of a mouse head, ((C)lateral view; (D) view from above), the confluence of sinuses, and the deep brain venous system (internal cerebral veins, Galeno vein, straight sinus, inferior sagittal sinus) can be easily appreciated as it resembles the configuration in humans. (from Mancini 2015 (82))

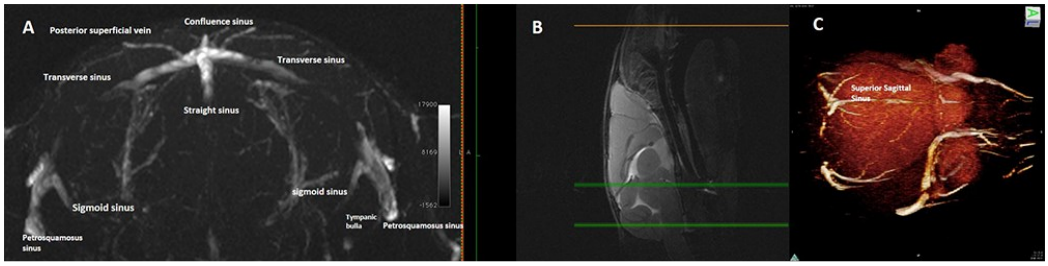

Fig 11. Magnetic resonance angiography with 3D of the confluence of sinuses and connections of the transverse sinuses. (A) Maximum Intensity Projection of axial Magnetic resonance angiography partitions, (B) at the occipito-cerebellar border (mid-sagittal T2w slice used as a reference), and (C) 3D rendering of magnetic resonance angiography acquisition of that region as seen from above. The confluence of sinuses and the connections of the Transverse sinuses are depicted. (from Mancini 2015 (82))

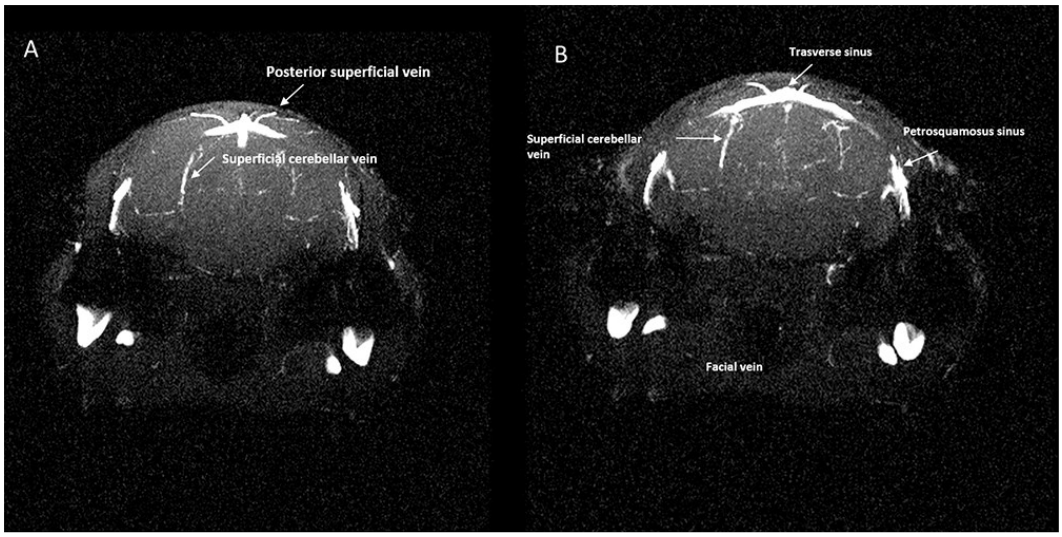

Fig 12. Magnetic resonance angiography of the transverse sinus. (A), (B), Single axial magnetic resonance angiography partitions at two levels showing (A) the tributaries of the transverse sinus and its lateral bifurcation into the straight sinus and (B) petrosquamosal sinus. (from Mancini 2015 (82))

The Inferior Sagittal Sinus (ISS) begins on the midline in the central part of the brain, runs parallel to the SSS deeper in the interhemispheric sulcus and joins caudally the Galeno vein (GV) (Figs 9A and 10C) to form the straight sinus. The TS, running along the posterior border the tentorium, receives the superior petrosal sinus, the posterior superficial cerebral vein and the superficial cerebellar veins (Figs 11 and 12). The TSs continue caudally and ventrally, on each side, near the petrosquamosal fissure, each of them bifurcating into two branches: the sigmoid sinus (SS) and the petrosquamosal sinus (Fig 13). The petrosquamosal sinus crosses the cranial bone, curves ventrally around the external margin of the timpanic bulla, and then emerges through the wide petrosquamosal fissure ("spurious" Jugular foramen), to run extracranially between the spurious jugular foramen and the temporomandibular joint and external auditory meatus (Fig 13E–13G). It divides into a branch that drains into the posterior facial vein and a branch that drains into the maxillary vein (Fig 13G). The micro-CT clearly demonstrated the relationship between the intracranial and extracranial veins with connection through three cranial foramina (Fig 13A–13G).

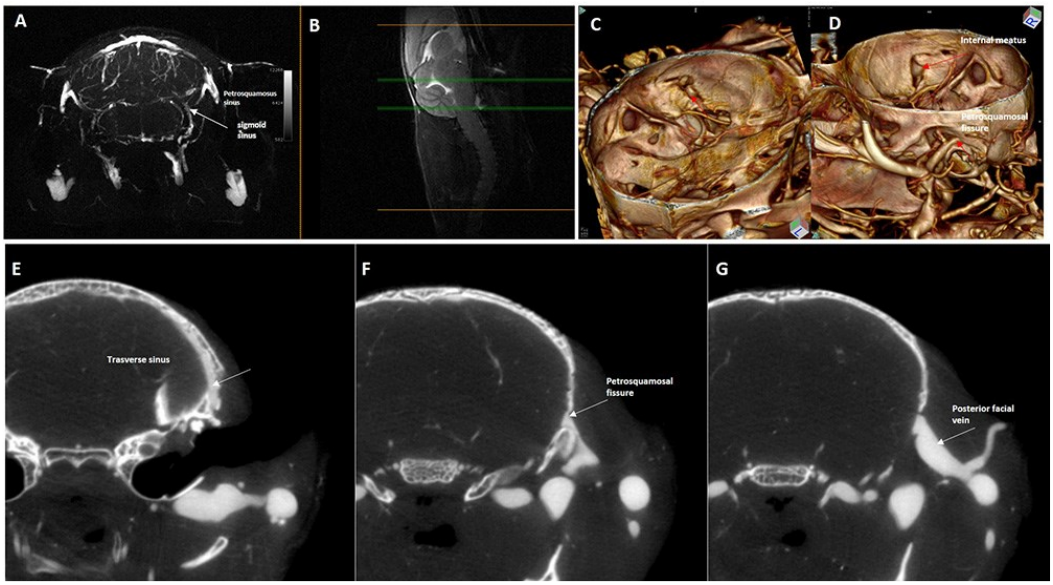

Fig 13. Magnetic resonance angiography with 3D rendering and silicon-computed tomography angiography of the petrosquamosal fissure. Upper row: Maximum Intensity Projection of axial magnetic resonance angiography partitions (slab at the occipito-cerebellar border (B) mid-sagittal T2w slice used as a reference,) and 3D rendering of silicon-enhanced computed tomography angiography as seen from (C) inside and (D) outside of the skull. (E), (F),(G) Lower row: Axial computed tomography slices in caudo-cranial sequence showing the exit from the brain of most of the transverse sinus blood through the petrosquamosal fissure (arrows), then joining the external jugular system. (from Mancini 2015 (82))

Intracranially, the TS continues in the SS that is a thin, atretic branch that runs dorsally around the medial border of tympanic bulla (Fig 11). The SS also receives the inferior petrosal sinuses and veins coming from the lateral aspect of pons and medulla and shows anastomoses with the vertebral venous plexus (Fig 13A), then crosses the jugular foramen, in the IJV. While running along the inner table of the posterior fossa, the TS receives the superior petrosal sinus, the caudal rhinal veins and the cerebellar veins (Fig 12A). As in humans, the deep system is composed by the internal cerebral veins (ICV), the basal vein, the Galeno vein (GV) and their tributaries. The GV (Fig 10) runs posteriorly along the interior–midline of the cerebrum, and receives the ICV together with the Rosenthal veins. The straight sinus drains the deep venous system through the GV as well as much of superficial venous system indirectly through the ISS. Posteriorly, the straight sinus empties into confluence sinuum (Fig 10), as in humans. The VVs collect the blood of the district of the midbrain, cerebellum and occipital plexus, and run together with the corresponding artery in the transverse foramen. The posterior

cranial fossa and cerebellum veins are also drained by the vertebral venous plexus.

Extra-cerebral and neck veins. The major venous output from the head is the EJV, which is formed at the junction of the posterior facial vein, the anterior facial vein, the maxillary vein and the superficial temporal vein on each side of the head (Fig 14). This vein then runs ventral to the clavicle into the thorax, converging with the internal jugular and subclavian veins into the ipsilateral superior vena cava. Posterior to the ocular bulb there is a large venous plexus (Fig 15A and 15B) that flows laterally in the posterior facial vein (Fig 15C and 15D). Small venous branches of the ophthalmic plexus run medially toward the region of the cavernous sinus. The cavernous sinus forms medially a large intercavernous sinus (Fig 16). The cavernous sinus drains into the superior petrosal sinus, which is divided into two branches, the largest crossing the cranial bone at the level of sphenoid bone (Fig 16H and 16I) and draining into the branches of the EJV, the smallest flowing downward into the SS. The cavernous sinus drains laterally along superior petrosal sinus to EJV and medially along the inferior petrosal sinus into the sigmoid-TS complex.

Fig 14. 3D magnetic resonance angiography of external jugular vein. 3D magnetic resonance angiography rendering of the extracranial vasculature as seen (A) in a frontal-inferior view and (B) in a lateral view. The main facial venous trunks are well-shown, running caudally to join together to form the external jugular vein. (from Mancini 2015 (82))

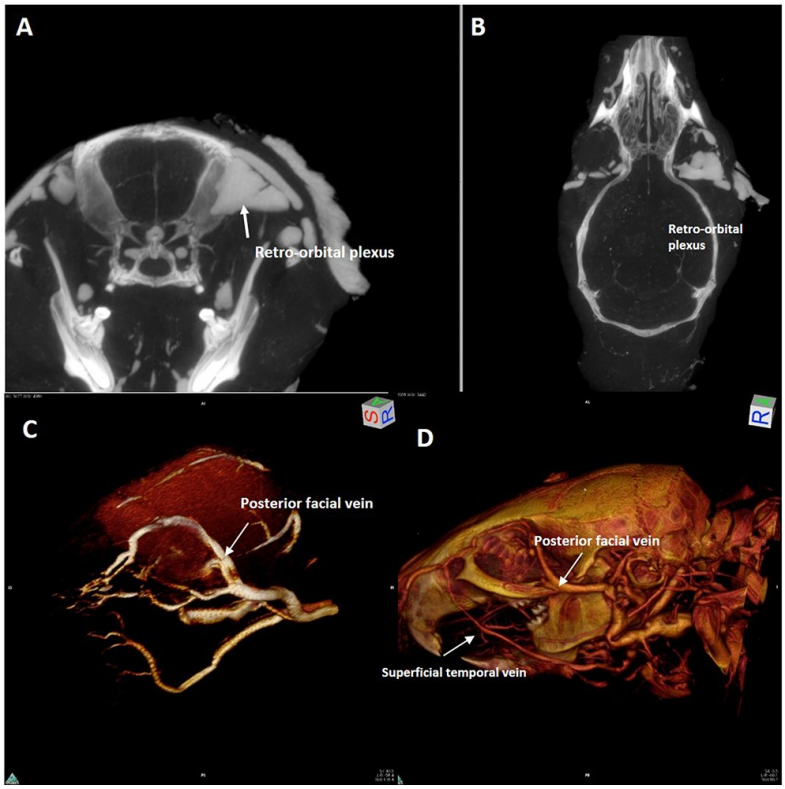

Fig 15. Magnetic resonance angiography with 3D rendering acquisition of the orbital region. Upper row: (A) axial and (B) coronal computed tomography slice. Lower row: 3D rendering of magnetic resonance angiography acquisition of the left orbital region ((C) antero-lateral view,). 3D rendering of silicon-enhanced computed tomography angiography ((D)lateral view,).(A), (B),The large retro-orbital venous plexus (white arrow) is clearly visible as well its drainage into the posterior facial vein ((C), (D) white arrow).(D)The superficial temporal vein is also shown in. (from Mancini 2015 (82))

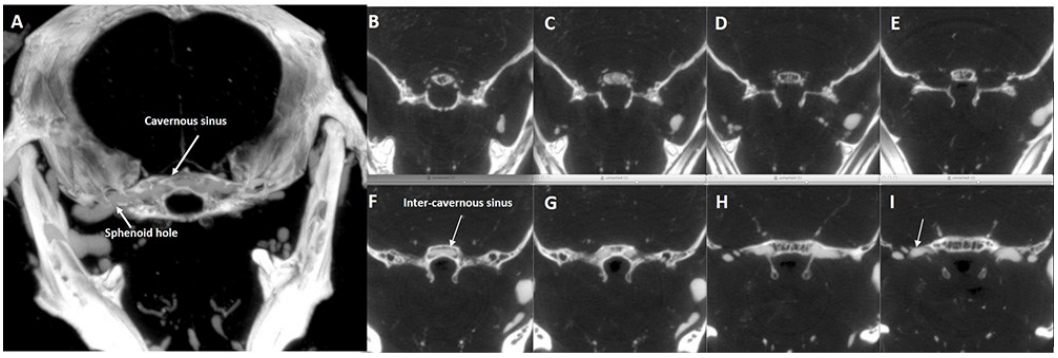

Fig 16. Axial computed tomography of the middle cranial fossa. Axial computed tomography slices at the level of the middle cranial fossa of the basicranium; (A) = 1mm-thick "MIP-ped" slab; (B)-(I) consecutive 0.05 mm-thick slices in a cranio-caudal sequence showing the confluence of small vessels in the hypothalamic region (B), (C), (D) toward a large intraosseus median inter-cavernous sinus (E), (F) which bilaterally exits the brain (G), (H) to join the external jugular vein system (arrow in (I)). (from Mancini 2015 (82))

The thin IJVs run in a typical position, anterior and lateral to the Carotid Artery (Figs 17 and 18), and drain the SSes (Fig 19), the occipital plexus (Fig 20) of the posterior cranial fossa and the cerebellar veins. EJV, IJV, and VVs have been insonated at different depths. The largest vein in the cervical region was the EJV that collects blood from the major part of the neck (Fig 21). The mean IJV diameter was 0.2 mm (200 μm) at the middle level of the neck, with a mean area of 0.08 mm^2, while the mean diameter and area for the EJV at the same level were 1.9 mm and 3 mm^2, respectively (Fig 21). The vein is not easily compressed; it is in a deep position, spaced from the surface by a thick layer of neck muscles. The cerebral blood flow appears to drain primarily into the EJV and VV and IJV and the flow could be collateralized. The waveform from different veins are presented in Fig 22A and 22B. The IJV is characterized by a low pulsatility waveform with a monophasic pattern and low pulsatility index. Conversely, EJV is characterized by three phasic pattern with high pulsatility, a small backflow component, resulting in high Pulsatility Index. Many collateral veins with anterior-posterior direction that were not identified in MRI and micro silicon-TC, were visible at Eco Color Doppler (ECD) (Fig 23).

Fig 17. Magnetic resonance angiography with 3D rendering of the neck vessels. 3D rendering of the magnetic resonance angiography acquisition of the neck vessels (right anterior oblique view), showing the external jugular vein, the internal jugular vein and the common carotid artery. (from Mancini 2015 (82))

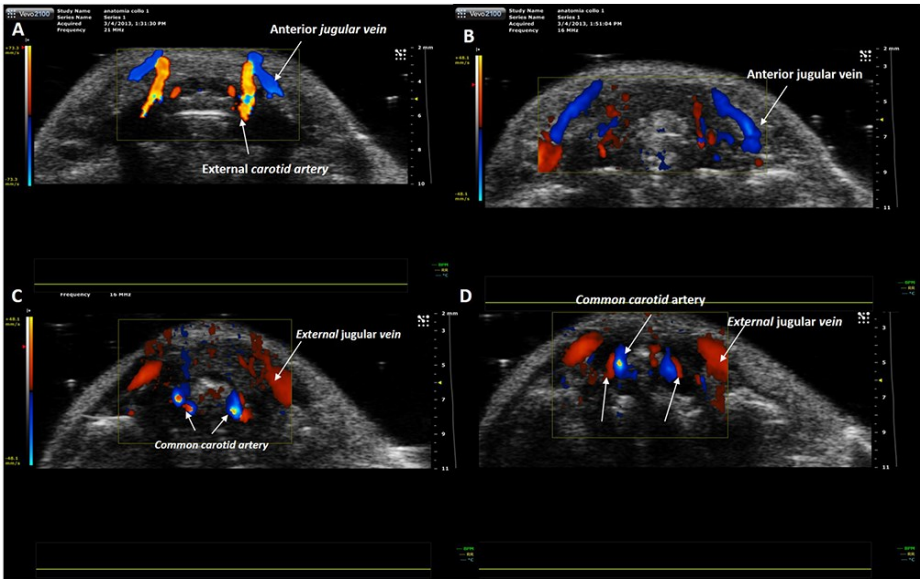

Fig 18. Eco-color Doppler examination. Craniocaudal scans performed with transverse planes of the upper and middle third of the mouse neck. (A) At the level of the upper third of the neck the external carotid artery runs anteriorly. (B-D) At level of middle third of the neck arterial and venous vessels are detectable. (B) The blood flow of anterior jugular veins is directed toward the external jugular veins. (C-D) The internal jugular veins are thin and in the typical position, anteriorly and laterally to the carotid artery. (from Mancini 2015 (82))

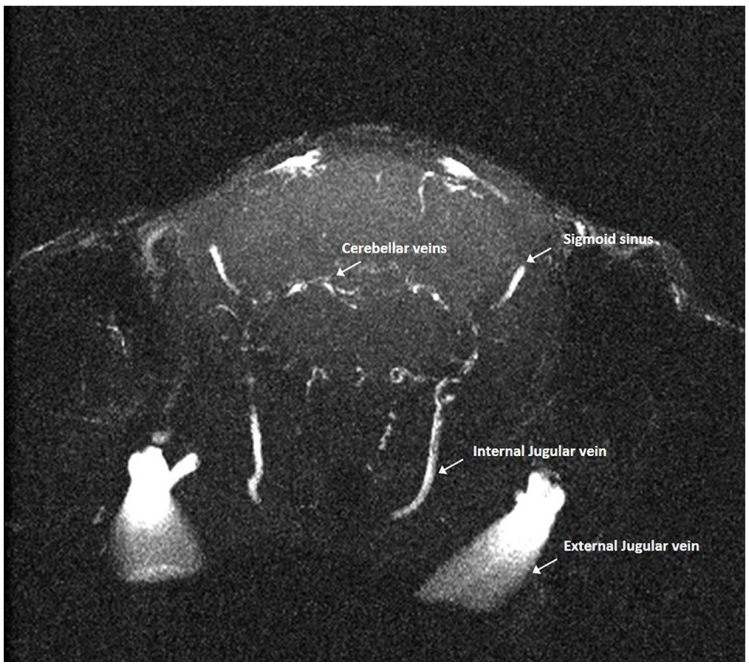

Fig 19. Magnetic resonance angiography of the internal jugular veins. Axial magnetic resonance angiography partitions at the level of the posterior cranial fossa showing some tributaries (e.g. cerebellar veins) of the internal jugular veins, which, differently from humans, is clearly hypotrophic in respect to the external jugular vein. (from Mancini 2015 (82))

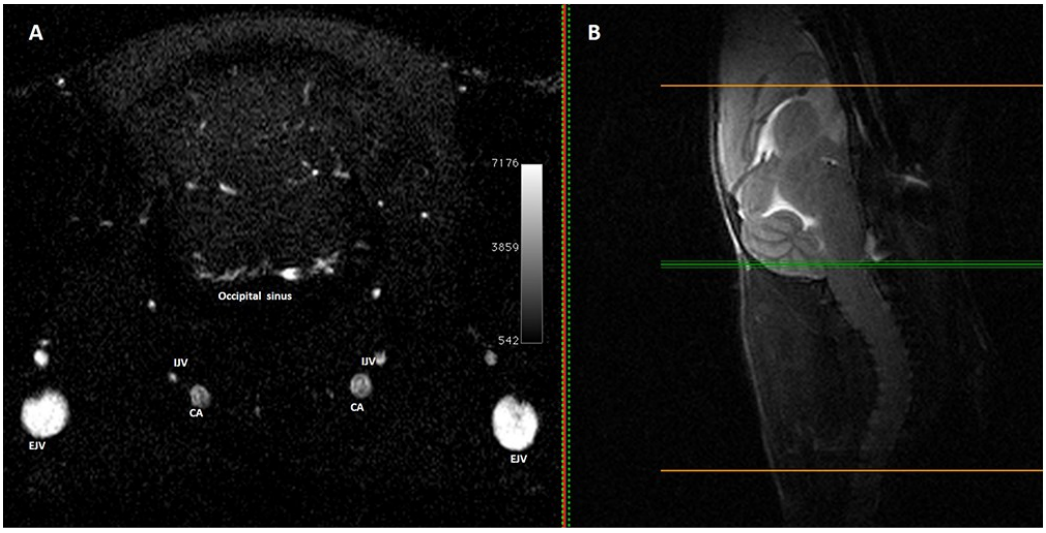

Fig 20. Magnetic resonance angiography of the lower part of the cerebellum and occipital plexus. (A) Single axial Magnetic resonance angiography partition at the level of the lower part of the cerebellum ((B) mid-sagittal T2w slice used as a reference) showing the occipital plexus. V: External Jugular Vein, IJV: Internal Jugular Vein, CA: Carotid Artery. (from Mancini 2015 (82))

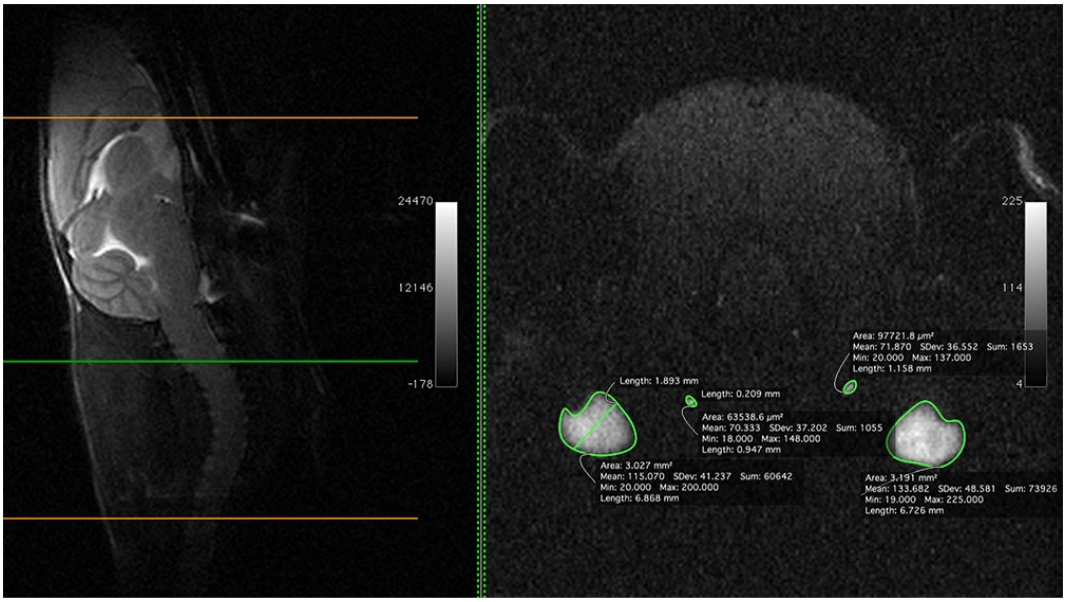

Fig 21. Magnetic resonance angiography of external jugular vein and internal jugular vein with size measurements. (B) Single axial magnetic resonance angiography partition at the middle level of the neck ((A) mid-sagittal T2w slice used as a reference,) showing the relative size (area, diameter, etc) of the external jugular vein and internal jugular vein. (from Mancini 2015 (82))

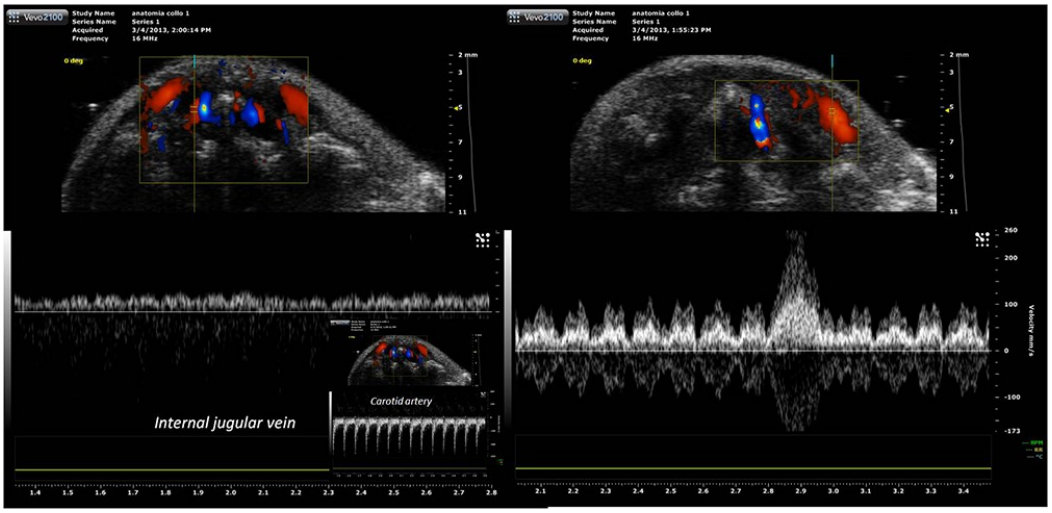

Fig 22. Eco-color doppler with pulsed doppler analysis of veins. (A)The internal jugular vein waveform is characterized by a monophasic pattern and low pulsatility index. (B)The external jugular vein is characterized by three-phasic pattern with high pulsatility. (C) In the small inset on the left the spectral analysis of the carotid artery blood flow is shown. (from Mancini 2015 (82))

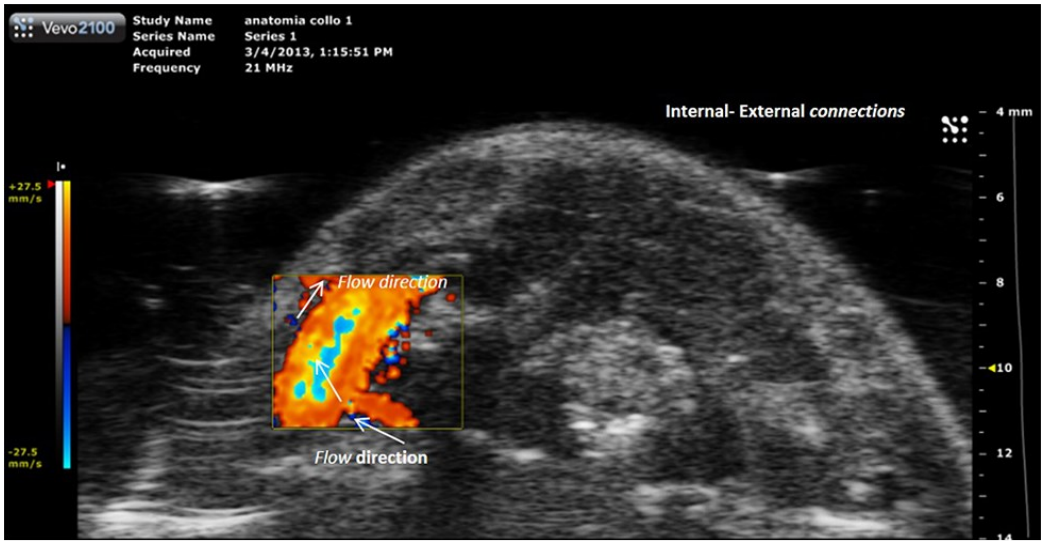

Fig 23. Eco-Color Doppler of vein collaterals. Collateral vein that connect external jugular vein and vertebral plexus. The flow is directed from vertebral plexus to the right external jugular vein. (from Mancini 2015 (82))

4.2.4 Discussion

Our observations on the mice anatomy of the cerebral veins confirm and more extensively describe the previous findings in rabbit and rats (87-91).

We have demonstrated the presence of a communication between facial veins, orbital veins and the cavernous system. As this interconnection system is valveless, blood can flow in any direction either to or from the brain. While animal models are invaluable research tools in helping us understand human diseases, in case of the cerebral venous system they are imperfect models for studying the human cerebral venous circulation. In mice the neck veins are always at the same level of the heart and, therefore, they are vessels with non- varying resistance, always open and constantly representing the major cerebral outflow pathway. Instead, in humans, the positioning of neck veins above heart level in upright position causes them to collapse, leading to an increased outflow resistance and to a cerebral outflow pathway that occurs predominantly through the vertebral venous plexus (16). It may be speculated that the intra-extracranial venous connections that we have demonstrated in the mouse could also represent a possible drainage pathway in the upright position in humans, partly explaining the remaining venous flow "mismatch" observed by Valdueza et al in 23 young healthy adults studied in supine and upright position by colour-coded duplex sonography, in whom the drop in jugular flow in the upright position was not adequately compensated by an increase in vertebral vein flow (56).

The pattern of the dorsal cranial venous system and deep venous system of the mouse is quite similar to the human (SSS, Rosenthal vein, GV, straight sinus, TSs and confluens sinuum). The TS runs between the temporo-mandibular joint and the external auditory meatus and drains into extracranial veins at the base of the skull. The SS drains in IJV, that is a tiny vessel and receives tributaries from cerebellum, occipital lobe and midbrain. The cavernous sinus passes through a foramen of the sphenoid bone, to join with the EJV. This demonstrates that the intracranial blood is predominantly drained by the extracranial district also for the drainage of cavernous sinus. The intracranial venous outflow runs in three directions: into the IJV and EJVs and into the vertebral venous plexus. Part of the venous drainage of the brain ultimately exits via the TS that is connected both

with EJV and IJV. Unlike humans, the EJVs predominate on the IJVs. The venous drainage of the mouse brain can be divided into two areas (Fig 24).

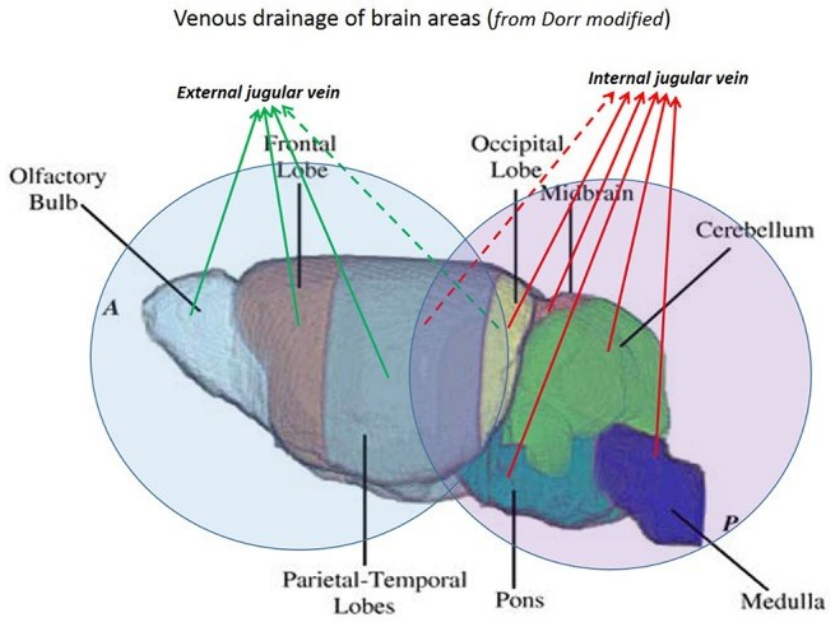

Fig.24 Cerebral areas with different venous drainage. Brain areas can be identified and divided according to the dominant venous drainage. The olfactory bulbs and frontal and parieto-temporal lobes drain mainly in the external jugular veins. The occipital lobe and cerebellum drain mainly in the internal jugular veins (modified from Dorr 2007 (92)).

Therefore, the interruption of EJV does not allow complete interruption of cerebral drainage with many possibilities of extra-intracranial collaterals. In a previous study, Atkinson et al (93)worked on establishing whether the EJV bilateral ligation can change the cerebral blood flow. They did not see any change in blood-brain barrier permeability, neuroinflammation, demyelination or clinical signs in Jugular Vein ligation compared to the changes in sham group. In our opinion, the use of mice as a vascular model for chronic venous hypertension is not plausible using a single vessel ligature. The use of mice vein ligature as animal model for cerebral venous stasis to understand the associated pathophysiology requires careful evaluation of mice vasculature and precise occlusion techniques, in order to successfully obstruct blood drainage from the brain. A large amount of blood flow is collected in the EJVs draining from the olfactory bulbs and from ocular tissues. Moreover, the venous system contains

connections between routes with potential collateralization. Therefore, if EJVs are occluded at the neck level many collateral pathways can compensate the venous hypertension. The use of mouse as a vascular model for chronic venous hypertension in humans is not plausible, unless it is demonstrated that no other drainage pathways are activated. Moreover, it is interesting to note that, at MRA, the SSS appeared thinner in its central part and wider both at its cranial and caudal end (i.e. at the connection with the rostral rhinal veins and at the confluence of sinuses, Fig 4C). This morphology suggest a possible bi-direction flow along its course, the blood flow being directed forward in the anterior part and backward in the posterior part. We thus assumed that, as in humans, the intracranial venous flow follows the large-scale gradient of vessel caliber. At the level of the neck veins, the flow direction was assessed by means of US color Doppler and showed the expected cranio-caudal direction. Among the limitations of the present work, one should consider that the injection/infusion of the silicon gel for CT angiography might lead to pathological deformation of the vascular system. In addition, the desirable saturation of arterial flow in the MRA acquisition of the venous system may lead to unwanted obscuration of the signal from venous tracts where flow speed and direction changes abruptly. We have provided a description of the cerebral venous drainage system of the mouse brain and neck. We identified many of the major branches and our result could be useful for future studies involving mouse cerebral veins. There are clear vascular differences between mouse and human anatomy.Three connections between intracranial and extracranial veins seem to be important drainage pathways of cerebral circulation in mouse and are absent in the humans were identified:

1. the petrosquamous sinus, already described in previous studies, that drains into the posterior facial vein.

2. the veins of the olfactory bulb, that drain in the superficial temporal vein through a foramen of the frontal bone.

3. the cavernous sinus, that drains in the EJV through a foramen of the sphenoid bone.

Chapter 5

Conclusion and Perspectives

We utilized CEUS to describe and quantify the IJV outflow in MS, CIS and HC. The main result was that MS patients showed, on average, approximately 30% reduction of the venous outflow through the IJV in supine position measured as WO rate percentage. These data are in agreement with other studies that showed impaired blood flow from the brain to the heart in patients with MS, with on average 63.5% higher hydraulic resistance of the cerebral-venous drainage system (94). Altered venous outflow was also demonstrated in other studies using MR imaging (95), Pletismography (75) and Flebography (96) in patients with Multiple Sclerosis associated with CCSVI, a condition characterized by impaired venous outflow from the central nervous system to the heart (45,97). The IJVs are the main drainage route for the cerebral venous system in supine position; in standing position these veins collapse and allow little blood flow. At steady-state the arterial inflow into the cranium must equal the venous outflow from the cranium. In MS patients the arterial inflow is preserved (98) since a reduction of venous outflow should result in an increase in the conduit's compliance, reduced flow pulsatility and increase outflow through collateral veins. Instead the upstream distention of the periventricular veins (99) is much more likely to be caused by constriction of the intracranial veins, perhaps by compression by inflammatory perivascular cuff. The association of IJV WO rate with EDSS score suggest that outflow changes could be related to MS disability and pathophysiology (100). The association of IJV TIC shapes and disease status is quite new in MS research and we believe that this simplified method might be useful to distinguish MS patients with or without associated vein outflow reduction/obstruction. Whereas arterial flow is tightly regulated and primarily controlled by metabolic demand, the lower blood pressure of the venous system makes venous flow more dependent on physiological conditions such as respiration and posture. The motor mechanisms of cerebral venous return are represented by the cardiac output, the so called vis a tergo, and by aspiration of the atrium and pleural cavity, or vis a fronte (4,56). The aspiration effect of the blood is a consequence of the negative pressure of the pleural cavity in inspiration (4). Such mechanism of aspiration determined by the

respiratory pump is particularly relevant in IJV. A raised pressure in the jugular veins could also be an earliest evidence of general systemic congestion, heart failure, hyperkinetic circulatory states, increased blood volume, bradycardia, increased intrapericardial, intrathoracic or intra-abdominal pressure, partial obstruction of the superior vena cava and tricuspid stenosis. Many investigators found reduced CBF in the GM and WM of patients with MS (101), in the deep grey matter the magnitude of CBF reduction increase with the severity of the disease (102) suggesting a continuum of decreased tissue perfusion, beginning in the withe matter and spreading to the grey matter as the disease progresses. Increased blood concentrations of the vasocostrictive compound endothelin-1 (ET-1) in patients with MS might also contribute to the slowdown of cerebral outflow (43). Although the ultrasound contrast agent used in this study is known to be not soluble in blood and the low mechanical index harmonic imaging technique was used to limit bubble destruction, some microbubbles may have been inherently destroyed during the 1-minute scanning that we have used. Therefore, the wash-out of microbubbles in the region of interest on contrast-enhanced sonography might have been exaggerated compared with the actual blood wash-out and with the contrast wash-out in CT or magnetic resonance perfusion studies. In conclusion, these results suggest that MS is associated with changes in the dynamics of the internal jugular vein.

To date, on the basis of available data is not possible know if the alteration of the cerebral venous outflow is primary cofactor of the cerebral alterations or secondary to endothelial dysfunction, alteration of respiratory and neck muscle.

The ultrasound method used is a quantitative method less operator dependent, overcoming methods currently used in clinical practice.

It would be desirable to verify the effect of venous obstruction in the brain of mouse on venous hemodynamic, however the mouse has many anatomical and physiological differences from humans.

In our animal study, many anatomical differences compared with humans were detected, therefore the use of mice as a vascular model for chronic venous hypertension is not plausible using a single vessel ligature. The use of mice vein

ligature as animal model for cerebral venous stasis to understand the associated pathophysiology requires careful evaluation of mice vasculature and precise occlusion techniques, in order to successfully obstruct blood drainage from the brain. A large amount of blood flow is collected in the EJVs draining from the olfactory bulbs and from ocular tissues. Moreover, the venous system contains connections between routes with potential collateralization. Therefore, if EJVs are occluded at the neck level many collateral pathways can compensate the venous hypertension. The use of mouse as a vascular model for chronic venous hypertension in humans is not plausible, unless it is demonstrated that no other drainage pathways are activated. This model can be used for other diseases involving the cerebral venous system.

Bibliography

1. O. Hassler, Deep cerebral venous system in man: a microangiographic study on its areas of drainage and its anastomoses with superficial cerebral veins, Neurology 16 (1966) 505–511.
2. J.F. Meder, J. Chiras, J. Roland, et al., Venous territories of the brain, J. Neuroradiol. 21 (1994) 118– 133.
3. J.P. Muizelaar, Cerebral blood flow, cerebral blood volume, and cerebral metabolism after severe head injury, in: D.P. Becker, S.K. Gudeman (Eds.), Textbook of Head Injury, WB Saunders, Philadelphia, PA, 1989, pp. 221–240.
4. B. Schaller Physiology of cerebral venous blood flow: from experimental data in animals to normal function in humans Brain Research Reviews 46 (2004) 243– 260.
5. M. Ono, A.L. Rhoton, D. Peace, et al., Microsurgical anatomy of the deep venous system of the brain, Neurosurgery 15 (1984) 621– 657
6. Einhaupl KM, Masuhr F.Cerebral Venous and Sinus thrombosis - an update Eur J Neurol 1994; 1: 109 - 26.
7. N.R. Mehta, L. Jones, M.A. Kraut, et al., Physiologic variations in dural venous sinus flow on phase-contrast MR imaging, Am. J. Roentgenol. 175 (2000) 221–225.
8. Anatomy of the human body, by Henry Gray. 20th ed., thoroughly rev. and re-edited by Warren H. Lewis. Gray's Anatomy 39th Edition, Elsevier
9. Kiliç T, Akakin A. Anatomy of cerebral veins and sinuses. Front Neurol Neurosci. 2008;23: 4-15.
10. Egan, Robert (2005) Anatomy and Physiology of the Cerebrovascular System Section 9: Chapter 39 Casey Eye Institute - Oregon Health and Science University Spencer S. Eccles Health Sciences Library.
11. Grand W, Hopkins LN. Vasculature of the brain and cranial base, variations in clinical anatomy. George Thieme Verlag. (1999) ISBN:0865777845

12. F Alpera et al "Importance of Anatomical Asymmetries of Transverse Sinuses: An MR Venographic Study" Cerebrovasc Dis 2004;18:236-239 (DOI: 10.1159/000079960)
13. Zivadinov R, Chung CP. Potential involvement of the extracranial venous system in central nervous system disorders and aging. BMC Med. 2013 Dec 17;11:260. doi: 10.1186/1741-7015-11-260
14. Harvey W. Cardiac Classics. St Louis: CV Mosby,1941:19.
15. Chih-Ping Chung, Han-Hwa Hu Jugular Venous Reflux J Med Ultrasound 2008;16(3):210–222Weissleder R., Wittenberg J. Neurological Imaging in Primer of Diagnostic Imaging, Third Edition. Philadelphia: Mosby 2003 : p 492.
16. Atkinson W, Forghani R, Wojtkiewicz GR, Pulli B, Iwamoto Y, Ueno T, et al. Ligation of the jugular veins does not result in brain inflammation or demyelination in mice. PLoS One 2012; 7(3):e33671. doi: 10. 1371/journal.pone.0033671 PMID: 22457780
17. Malferrari G, Zedde M, Prati P. Neurosonological Evaluation of Cerebral Venous Outflow, Springer, 2014.
18. Weinshenker BG, Bass B, Rice GP, Noseworthy J, CarriereW, Baskerville J, et al. The natural history ofmultiple sclerosis: a geographically based study. I. Clinical course and disability. Brain 1989;112(Pt 1):133–46.
19. Haussleiter IS, Brune M, Juckel G. Psychopathology in multiple sclerosis: diagnosis, prevalence and treatment. Ther Adv Neurol Disord 2009;2:13–29.
20. Young CA. Factors predisposing to the development of multiple sclerosis. QJM 2011;104:383–6.
21. Marrie RA. Environmental risk factors inmultiple sclerosis aetiology. Lancet Neurol 2004;3:709–18.
22. van der Mei IA, Simpson Jr S, Stankovich J, Taylor BV. Individual and joint action of environmental factors and risk of MS. Neurol Clin 2011;29:233–55.

23. Tettey P, Simpson S Jr, Taylor BV, van der Mei IA. Vascular comorbidities in the onset and progression of multiple sclerosis. J Neurol Sci. 2014 Dec 15;347(1-2):23-33. doi: 10.1016/j.jns.2014.10.020. Epub 2014 Oct 16.
24. D'haeseleer M, Cambron M, Vanopdenbosch L, De Keyser J. Vascular aspects of multiple sclerosis. Lancet Neurol. 2011 Jul;10(7):657-66. doi: 10.1016/S1474-4422(11)70105-3.
25. Koch-Henriksen N, Bronnum-Hansen H, Stenager E. Underlying cause of death in Danish patients with multiple sclerosis: results from the Danish Multiple Sclerosis Registry. J Neurol Neurosurg Psychiatry 1998; 65: 56–59.
26. Bronnum-Hansen H, Koch-Henriksen N, Stenager E. Trends in survival and cause of death in Danish patients with multiple sclerosis. Brain 2004; 127: 844–50
27. Allen NB, Lichtman JH, Cohen HW, Fang J, Brass LM, Alderman MH. Vascular disease among hospitalized multiple sclerosis patients. Neuroepidemiology 2008; 30: 234–38.
28. Christiansen CF, Christensen S, Farkas DK, Miret M, Sorensen HT, Pedersen L. Risk of arterial cardiovascular diseases in patients with multiple sclerosis: a population-based cohort study.
29. Ross R. Atherosclerosis—an inflammatory disease. N Engl J Med 1999; 340: 115–26.
30. Ridker PM, Hennekens CH, Buring JE, Rifai N. C-reactive protein and other markers of infl ammation in the prediction of cardiovascular disease in women. N Engl J Med 2000; 342: 836–43.
31. Sitia S, Tomasoni L, Atzeni F, et al. From endothelial dysfunction to atherosclerosis. Autoimmun Rev 2010; 9: 830–34.
32. Minagar A, Jy W, Jimenez JJ, et al. Elevated plasma endothelial microparticles in multiple sclerosis. Neurology 2001; 56: 1319–24.
33. Aksungar FB, Topkaya AE, Yildiz Z, Sahin S, Turk U. Coagulation status and biochemical and infl ammatory markers in multiple sclerosis. J Clin Neurosci 2008; 15: 393–97.
34. Cai H, Harrison DG. Endothelial dysfunction in cardiovascular diseases: the role of oxidant stress. Circ Res 2000; 87: 840–44.

35. Sahin S, Aksungar FB, Topkaya AE, et al. Increased plasma homocysteine levels in multiple sclerosis. Mult Scler 2007; 13: 945–46.
36. Russo C, Morabito F, Luise F, et al. Hyperhomocysteinemia is associated with cognitive impairment in multiple sclerosis. J Neurol 2008; 255: 64–69.
37. Ramsaransing GS, Fokkema MR, Teelken A, Arutjunyan AV, Koch M, De Keyser J. Plasma homocysteine levels in multiple sclerosis. J Neurol Neurosurg Psychiatry 2006; 77: 189–92.
38. He L, Zeng H, Li F, et al. Homocysteine impairs coronary artery endothelial function by inhibiting tetrahydrobiopterin in patientswith hyperhomocysteinemia. Am J Physiol Endocrinol Metab 2010; 299: E1061–65.
39. Sekula M, Janawa G, Stankiewicz E, Stepien E. Endothelial microparticle formation in moderate concentrations of homocysteine and methionine in vitro. Cell Mol Biol Lett 2011;16: 69–78.
40. Wuerfel J, Paul F, Zipp F. Cerebral blood perfusion changes in multiple sclerosis. J Neurol Sci 2007; 259: 16–20.
41. Law M, Saindane AM, Ge Y, et al. Microvascular abnormality in relapsing-remitting multiple sclerosis: perfusion MR imaging findings in normal-appearing white matter. Radiology 2004; 231: 645–52.
42. Adhya S, Johnson G, Herbert J, et al. Pattern of hemodynamic impairment in multiple sclerosis: dynamic susceptibility contrast perfusion MR imaging at 3.0 T. Neuroimage 2006; 33: 1029–35.
43. Haufschild T, Shaw SG, Kesselring J, Flammer J. Increased endothelin-1 plasma levels in patients with multiple sclerosis. J Neuroophthalmol 2001; 21: 37–38.
44. Speciale L, Sarasella M, Ruzzante S, et al. Endothelin and nitric oxide levels in cerebrospinal fluid of patients with multiple sclerosis. J Neurovirol 2000; 6 (suppl 2): S62–66.
45. Zamboni P, Galeotti R, Menegatti E, et al. Chronic cerebrospinal venous insufficiency in patients with multiple sclerosis. J Neurol Neurosurg Psychiatry 2009; 80: 392–99.
46. Zamboni P, Galeotti R. The chronic cerebrospinal venous insufficiency syndrome. Phlebology 2010; 25: 269–79

47. Doepp F, Paul F, Valdueza JM, Schmierer K, Schreiber SJ. No cerebrocervical venous congestion in patients with multiple sclerosis. Ann Neurol 2010; 68: 173–83.
48. Krogias C, Schröder A, Wiendl H, Hohfeld R, Gold R. Chronic cerebrospinal venous insuffi ciency and multiple sclerosis: critical analysis and fi rst observation in an unselected cohort of MS patients. Nervenartz 2010; 81: 740–46.
49. Mayer CA, Pfeilschifter W, Lorenz MW, et al. The perfect crime? CCSVI not leaving a trace in MS. J Neurol Neurosurg Psychiatry 2011; 82: 436–40.
50. Baracchini C, Perini P, Calabrese M, Causin F, Rinaldi F, Gallo P. No evidence of chronic cerebrospinal venous insuffi ciency at multiple sclerosis onset. Ann Neurol 2011; 69: 90–99.
51. Beggs C. Multiple sclerosis appears to be associated with cerebral venous abnormalities. Ann Neurol 2010; 68: 560–61; author reply 561–62.
52. Sundström P, Wahlin A, Ambarki K, Birgander R, Eklund A, Malm J. Venous and cerebrospinal fluid flow in multiple sclerosis: a case-control study. Ann Neurol 2010; 68: 255–59.
53. Singh AV, Zamboni P. Anomalous venous blood flow and iron deposition in multiple sclerosis. J Cereb Blood Flow Metab 2009; 29: 1867–78.
54. Menegatti E, Zamboni P. Doppler haemodynamics of cerebral venous return. Curr Neurovasc Res. 2008 Nov;5(4):260-5.
55. San Millan Ruiz, D, Gailloud, P, Rufenacht, DA, Delavelle, J, Henry, F, Fasel, JH., (2002) The craniocervical venous system in relation to cerebral venous drainage. Am J Neuroradiol 23: 1500-8.
56. Valdueza, JM, von Munster, T, Hoffman, O, Schreiber, S, Einhaupl, KM. (2000) Postural dependency of the cerebral venous outflow. Lancet 355: 200-201.
57. Gisolf, J, van Lieshout, JJ, van Heusden, K, Pott, F, Stok, WJ, Karemaker, JM. (2004) Human cerebral venous outflow pathway depends on posture and central venous pressure. J Physiol 560: 317-27

58. Schreiber, SJ, Lurtzing, F, Gotze, R, Doepp, F, Klingebiel, R, Valdueza, JM. (2003) Extrajugular pathways of human cerebral venous blood drainage assessed by duplex ultrasound. J Appl Physiol 94:1802-1805
59. Doepp, F, Schreiber, SJ, von Münster, T, Rademacher, J, Klingebiel, R, Valdueza, JM. (2004) How does the blood leave the brain? A systematic ultrasound analysis of cerebral venous drainage patterns. Neuroradiology 46: 565-70.
60. Nicolaides, AN, and the International Consensus Group. (2000) "The investigation of chronic venous insufficiency. A Consensus Statement". Circulation 102: 126-163.
61. Coleridge-Smith, P, Labropoulos, N, Partsch, H, Myers, K, Nicolaides, A, Cavezzi, A. (2006) Duplex ultrasound investigation of the veins in chronic venous disease of the lower limbs--UIP consensus document. Part I. Basic principles. Eur J Vasc Endovasc Surg 31: 83-92.
62. Folkow, B, Neil, E. (1973) Circulation. Oxford University Press, New York pp. 10-11
63. Lichtenstein, D, Saïfi, R, Augarde, R, Prin, S, Schmitt, JM, Page, B, Pipien, I, Jardin, F. (2001) The internal jugular veins are asymmetric. Usefulness of ultrasound before catheterization. Intensive Care Med 27: 301-5.
64. Zamboni, P, Portaluppi, F, Marcellino, M.G, Quaglio, D, Manfredini, R, Liboni, A, Stoney, RJ. (1998): In vitro > in vivo assessment of vein wall properties. Ann Vasc Surg 12: 324-329.
65. Zamboni, P, Portaluppi, F, Marcellino, M.G, Pisano, L, Manfredini, R, Liboni A. (1997) Ultrasonographic assessment of ambulatory venous pressure in superficial venous incompetence. J Vasc Surg 26: 796-780.
66. Delorme S, Krix M. Contrast-enhanced ultrasound for examining tumor biology. Cancer Imaging 2006;6:148–152.
67. Bateman GA (2002) Pulse-wave encephalopathy: a comparative study of the hydrodynamics of leukoaraiosis and normal-pressure hydrocephalus. Neuroradiology, 44:740–748.
68. Digre KB (2002) Idiopathic intracranial hypertension headache. Curr Pain Headache Rep 6:217–225.

69. Doepp F, Ba¨hr D, John M, Hoernig S, Valdueza JM (2008) Internal jugular vein valve incompetence in COPD and primary pulmonary hypertension. J Clin Ultrasound 36(8): 480–484.
70. Doepp F, Valdueza JM, Schreiber SJ (2008) Incompetence of internal jugular valve in patients with primary exertional headache: a risk factor? Cephalalgia 28 (2):182–185.
71. Chung CP, Hu HH (2010) Pathogenesis of leukoaraiosis: role of jugular venous reflux. Med Hypotheses 75: 85–90.
72. Chung CP, Wang PN, Wu YH, Tsao YC, Sheng WY, et al. (2011) More severe white matter changes in the elderly with jugular venous reflux Ann Neurol 69:553–559
73. Zivadinov R, Marr K, Cutter G, Ramanathan M, Benedict RH, et al. (2011) Prevalence, sensitivity, and specificity of chronic cerebrospinal venous insufficiency in MS. Neurology 77: 138–144.
74. Mancini M, Lanzillo R, Liuzzi R, Di Donato O, Ragucci M, Monti S, Salvatore E, Morra VB, Salvatore M. Internal jugular vein blood flow in multiple sclerosis patients and matched controls. PLoS One. 2014 Mar 27;9(3):e92730. doi: 10.1371/journal.pone.0092730. eCollection 2014.
75. Beggs C, Shepherd S, Zamboni P (2013) Cerebral venous outflow resistance and interpretation of cervical plethysmography data with respect to the diagnosis of chronic cerebrospinal venous insufficiency Phlebology, phleb.2012.012039, first published on May 3
76. Denislic M, Milosevic Z, Zorc M, Ravnik IZ, Mendiz O (2013) Disability caused by multiple sclerosis is associated with the number of extracranial venous stenoses: possible improvement by venous angioplasty. Results of a prospective study. Phlebology 28:353–360
77. Weinstock-Guttman B, Ramanathan M, Marr K, Hojnack D, Benedict RH, et al. (2012) Clinical correlates of chronic cerebrospinal venous insufficiency in multiple sclerosis. BMC Neurol 2012, 12:26
78. Gosselink R, Kovacs L, Decramer M (1999) Respiratory muscle involvement in multiple. Eur Respir J 13: 449–454
79. Gianesini S, Menegatti E, Mascoli F, Salvi F, Bastianello S, et al. (2013) The omohyoid muscle entrapment of the internal jugular vein. A still

unclear pathogenetic mechanism. Phlebology [Epub ahead of print] doi:10.1177/0268355513489549

80. Dolic K, Marr K, Valnarov V, Dwyer MG, Carl E, et al. (2012) Intra- and Extraluminal Structural and Functional Venous Anomalies in Multiple Sclerosis, as Evidenced by 2 Noninvasive Imaging Techniques. AJNR Am J Neuroradiol 33(1):16–23.
81. Jayaraman MV, Boxerman JL, Davis LM, Haas RA, Rogg JM (2012) Incidence of extrinsic compression of the internal jugular vein in unselected patients undergoing CT angiography. AJNR Am J Neuroradiol 33(7):1247–1250.
82. Mancini M, Greco A, Tedeschi E, Palma G, Ragucci M, Bruzzone MG, Coda AR, Torino E, Scotti A, Zucca I, Salvatore M. Head and Neck Veins of the Mouse. A Magnetic Resonance, Micro Computed Tomography and High Frequency Color Doppler Ultrasound Study. PLoS One. 2015 Jun 11;10(6):e0129912. doi: 10.1371/journal.pone.0129912. eCollection 2015.
83. Dorr AE, Lerch JP, Spring S, Kabani N, Henkelman RM. High resolution three-dimensional brain atlas using an average magnetic resonance image of 40 adult C57Bl/6J mice. Neuroimage 2008; 42(1):60–69; doi: 10.1016/j.neuroimage.2008.03.037 PMID: 18502665
84. Pathak AP, Kim E, Zhang J, Jones MV. Three-dimensional imaging of the mouse neurovasculature with magnetic resonance microscopy. PLoS One 2011; 6(7):e22643; doi: 10.1371/journal.pone. 0022643 PMID: 21818357
85. Weyers J, Carlson DD, Murry CE, Schwartz SM, Mahoney WM Jr. Retrograde perfusion and filling of mouse coronary vasculature as preparation for micro computed tomography imaging. J Vis Exp 2012; (60:):e3740; doi: 10.3791/3740 PMID: 22353785
86. Ghanavati S, Yu LX, Lerch JP, Sled JG. A perfusion procedure for imaging of the mouse cerebral vasculature by X-ray micro-CT. J Neurosci Methods. 2014 Jan 15; 221:70–7. doi: 10.1016/j.jneumeth. 2013.09.002 PMID: 24056228
87. Scremin OU, Sonnenschein RR, Rubinstein EH. Cerebrovascular anatomy and blood flow measurements in the rabbit. J Cereb Blood Flow Metab 1982; 2(1):55–66. PMID: 7061603

88. Jeppsson PG, Olin T. Cerebral angiography in the rabbit. An investigation of vascular anatomy and variation in circulatory patterns with conditions of injection. Lund Univ Arsskr NF Avd 1960; 256(14):1–56.
89. Szabó K. The cranial venous system in the rat: anatomical pattern and ontogenetic development. I. Basal drainage. Anat Embryol (Berl) 1990; 182(3):225–234. PMID: 2268066
90. Hofmann M. Zur vergleichenden Anatomie der Gehirn und Rückenmarksarterien der Vertebraten. Z. Morph. Antrop. 1900; 2: 247–320.
91. Krause W. Die Anatomie des Kaninchens in Topographischer und Operativer Riicksicht. Leipzig, Engelmann 1884.
92. Dorr A, Sled JG, Kabani N. Three-dimensional cerebral vasculature of the CBA mouse brain: A magnetic resonance imaging and micro computed tomography study. NeuroImage 2007; 35:1409–1423. PMID: 17369055
93. Atkinson W, Forghani R, Wojtkiewicz GR, Pulli B, Iwamoto Y, Ueno T, et al. Ligation of the jugular veins does not result in brain inflammation or demyelination in mice. PLoS One 2012; 7(3):e33671. doi: 10. 1371/journal.pone.0033671 PMID: 22457780
94. Zamboni P, Menegatti E, Conforti P, Shepherd S, Tessari M, et al. (2012) Assessment of cerebral venous return by a novel plethysmography method. J Vasc Surg, 56:677–685.
95. Haacke EM, Feng W, Utriainen D, Trifan G, Wu Z, et al. (2012) Patients with multiple sclerosis with structural venous abnormalities on MR imaging exhibit an abnormal flow distribution of the internal jugular veins. J Vasc Interv Radiol. 23:60–68.
96. Veroux P, Giaquinta A, Perricone D, Lupo L, Gentile F, et al. (2013) Internal jugular veins out flow in patients with multiple sclerosis:a catheter venography study. J Vasc Interv Radiol. 24(12):1790–7
97. Zamboni P, Menegatti E, Galeotti R, Malagoni AM, Tacconi G, et al. (2009) The value of cerebral Doppler venous haemodynamics in the assessment of multiple sclerosis. J Neurol Sci 282(1-2): 21–27
98. Mancini M, Morra VB, Di Donato O, Maglio V, Lanzillo R, et al. (2012) Multiple sclerosis: cerebral circulation time. Radiology 262(3):947–955.

99. Gaitan MI, de Alwis MP, Sati P, Nair G, Reich DS (2013) Multiple sclerosis shrinks intralesional, and enlarges extralesional, brain parenchymal veins. Neurology 80 145–151.

100. Lanzillo R, Mancini M, Liuzzi R, Di Donato O, Salvatore E, et al. (2013). Chronic cerebrospinal venous insufficiency in Multiple Sclerosis: an highly prevalent age-dependent phenomenon. BMC Neurology, 13–20 doi:10.1186/ 1471-2377-13-20

101. Ge Y, Law M, Johnson G, Herbert J, Babb JS, et al. (2005) Dynamic susceptibility contrast perfusion MR imaging of multiple sclerosis lesions: characterizing hemodynamic impairment and inflammatory activity. AJNR Am J Neuroradiol 26:1539–1547.

102. Inglese M, Adhya S, Johnson G, Babb JS, Miles L, et al. (2008) Perfusion magnetic resonance imaging correlates of neuropsychological impairment in multiple sclerosis. J Cereb Blood Flow Metab 28:164–171

Acknowledgements

The research work on which this thesis is based has been performed during my stay at the Institute of Biostructures and Bioimaging - National Research Council of Italy, Naples, Italy. I would like to express my deepest thanks to my two supervisors, Prof. Marcello Mancini and Prof. Simone Maurea. I would like to express my sincere gratitude to Prof Marcello Mancini for the continuous support of my Ph.D study and related research, for his patience, motivation, and immense knowledge. His guidance helped me in all the time of research and writing of this thesis. I want to thank Prof. Simone Maurea for his support and encouragement. His advice and its availability have been for me a great help during the PhD study. I wish to express my gratitude to the Collegio dei Docenti del Dottorato di Ricerca in Imaging Molecolare, and to Prof. Alberto Cuocolo, for giving me the chance to pursue my research studies. Finally, I would like to thank the institution of University of Naples "Federico II" that, during the three years of doctoral studies, has provided me with the necessary financial support.